

Impact of Diurnal Warm Layers on Atmospheric Convection

Radomyra Shevchenko¹, Cathy Hohenegger¹, and Mira Schmitt²

¹Max Planck Institute for Meteorology

²Leibniz Institute for Baltic Sea Research

January 17, 2023

Abstract

This manuscript presents a study of oceanic diurnal warm layers in kilometer-scale global coupled simulations and their impact on atmospheric convection in the tropics. With the implementation of thin vertical levels in the ocean, diurnal warm layers are directly resolved, and sea surface temperature (SST) fluctuations of up to several Kelvin appear in regions with low wind and high solar radiation. The increase of SST during the day causes an abrupt afternoon increase of atmospheric moisture due to enhanced latent heat flux, followed by an increase in cloud cover and cloud liquid water. However, although the daily SST amplitude is exaggerated in comparison to reanalysis, this effect only lasts for 5-6 hours and leads to an absolute difference of 1% for cloud cover and 0.01 kg m⁻² for cloud liquid water. All in all, the impact of diurnal warm layers on convective cloud cover is found to be negligible in the tropical mean.

1
2
3
4
5
6
7
8
9
10
11

Impact of Diurnal Warm Layers on Atmospheric Convection

Radomyra Shevchenko¹, Cathy Hohenegger¹, and Mira Schmitt²

¹Max Planck Institute for Meteorology, Hamburg, Germany
²Leibniz Institute for Baltic Sea Research, Warnemünde, Germany

Key Points:

- Diurnal warm layers increase atmospheric moisture.
- The increase of cloud cover following the formation of a diurnal warm layer is immediate and only lasts for several hours.
- The magnitude of the cloud cover increase is small and has no discernible influence on the global mean.

Corresponding author: Radomyra Shevchenko, radomyra.shevchenko@mpimet.mpg.de

Abstract

This manuscript presents a study of oceanic diurnal warm layers in kilometer-scale global coupled simulations and their impact on atmospheric convection in the tropics. With the implementation of thin vertical levels in the ocean, diurnal warm layers are directly resolved, and sea surface temperature (SST) fluctuations of up to several Kelvin appear in regions with low wind and high solar radiation. The increase of SST during the day causes an abrupt afternoon increase of atmospheric moisture due to enhanced latent heat flux, followed by an increase in cloud cover and cloud liquid water. However, although the daily SST amplitude is exaggerated in comparison to reanalysis, this effect only lasts for 5-6 hours and leads to an absolute difference of 1% for cloud cover and 0.01 kg m^{-2} for cloud liquid water. All in all, the impact of diurnal warm layers on convective cloud cover is found to be negligible in the tropical mean.

Plain Language Summary

The daily fluctuations of sea surface temperature (SST) have been extensively studied for the last decades, but the assessment of importance of this phenomenon for atmospheric convection on the global scale has come within reach only very recently, thanks to the development of simulations with a horizontal resolution of $O(1 \text{ km})$. In this manuscript we show that we can indeed observe an impact of SST fluctuations on moisture in the atmosphere. However, the impact on the amount of cloud in the tropics is found to be short-lived and its magnitude negligible on average.

1 Introduction

Diurnal sea surface temperature anomalies and their interplay with the atmosphere and in particular with the diurnal cycle of convection have been an object of study for many decades. In this study, we investigate this connection for the first time using simulations that can explicitly resolve both the daily temperature variations in the ocean and convection in the atmosphere on a global scale.

Daily variations in sea surface temperature (SST) have already been described in Sverdrup et al. (1942). Since then, there have been numerous studies describing the physics and the conditions of appearance of daily sea surface temperature (SST) variations, the seminal work by Price et al. (1986) being the first detailed description of this phenomenon. Under low-wind conditions and with sufficient insolation, a stable near-surface layer forms during the day in the upper layers of the ocean (until the depth of $O(10 \text{ m})$) that leads to a surface warming of up to 5 K (see Wick and Castro (2020)). In absence of solar radiation during the night, the stratification dissolves as vertical turbulent mixing takes overhand, until a homogeneous mixed layer is restored. The physics of this phenomenon is described in detail in a monograph by Soloviev and Lukas (2013). This stratified, warm layer is known as diurnal warm layer (DWL) and it is ubiquitous in all latitudes, causing SST fluctuations of 0.2 K or more in the entire Northern hemisphere and beyond during boreal summer (see Gentemann et al. (2003)). A comprehensive discussion of its definition and properties can be found in a review by Kawai and Wada (2007). In particular, the authors of the review point out that the presence of DWLs in observations as well as in single column simulations leads to stronger latent and sensible heat fluxes. As surface fluxes connect the surface to the atmospheric boundary layer and since changes in boundary layer properties affect the development of convection, the question of the impacts of DWLs on atmospheric convection arises.

Investigating this question in models requires both fine enough vertical resolution in the ocean, to resolve DWLs, and fine enough horizontal grid spacing in the atmosphere, to resolve atmospheric convection. With the development of deca- to kilometer scale simulations in a coupled configuration such investigations are becoming possible. Prominent

61 among the newest studies are the papers by Voldoire et al. (2022) and Brilouet et al. (2021).
 62 In Voldoire et al. (2022), a single column coupled model has been considered, while in
 63 Brilouet et al. (2021), a one column ocean model has been coupled to an atmospheric
 64 large-eddy simulation model integrated over a limited area. Both experiments are based
 65 on or validated with the data from the Dynamics of the Madden Julian Oscillation (DY-
 66 NAMO) campaign, during which daily SST differences of several Kelvin were observed.
 67 Voldoire et al. (2022) showed that the impact of DWLs on the boundary layer depth,
 68 atmospheric moisture and precipitation seems to be small. In contrast, de Szoeke et al.
 69 (2021) argued that in the observations from the DYNAMO data set, convection is en-
 70 hanced on days with large SST differences. Finally, Voldoire et al. (2022) conjectured
 71 that a single column model cannot capture horizontal interactions that might lead to a
 72 larger impact.

73 To the authors' knowledge, there is yet no study extending the question of inter-
 74 actions between DWLs and atmospheric convection to a realistic, global framework with
 75 resolved convection. And yet, atmospheric convection plays a key role in the energy and
 76 water cycle in the tropics, therefore describing the driving mechanisms of convection and
 77 assessing their importance is crucial.

78 The present study aims at closing this gap and precisely analysing the impact of
 79 DWLs on atmospheric convection in a global, coupled ICON simulation with 5km hor-
 80 izontal resolution and decameter grid spacing in the first oceanic layers. This allows us
 81 to resolve DWL and convection, to assess their interactions, also by resolving horizon-
 82 tal gradients, and to analyse the global impacts of DWLs. We are particularly interested
 83 in understanding whether the presence of DWLs enhances cloud cover in a time frame
 84 of several days and if so, whether this happens through a direct moistening by the la-
 85 tent heat flux or by enhancing spatial gradient in SST and mesoscale circulations. More-
 86 over, the global nature of our simulation allows to zoom in on different areas and encom-
 87 pass other meteorological and sea conditions than the ones of the DYNAMO campaign.

88 The manuscript is structured as follows. In Section 2 we describe the setup of the
 89 experiments, and in Section 3 we analyse the representation and properties of DWLs in
 90 global ICON simulations. In Section 4 we quantify the effect of DWLs on surface fluxes,
 91 atmospheric moisture and clouds, and finally in Section 5 we present the conclusions of
 92 our work.

93 2 Experimental setup

94 To study the effect of DWLs, we conduct global coupled simulations with the ICON
 95 model in its Sapphire configuration. The Sapphire configuration targets simulations with
 96 a horizontal grid spacing finer than 10 km. For our simulations, we use a setup similar
 97 to the simulation called `G_A0_5km` in Hohenegger et al. (2022), with small deviations that
 98 will be described below. The model is fully coupled, and at the horizontal resolution of
 99 approximately 5 km it is at the boundary of resolving convection. Although the cloud
 100 amount associated with shallow convection is expected to be overestimated (see Vial et
 101 al. (2019) and Hohenegger et al. (2020)), it has been demonstrated in Vial et al. (2019)
 102 that both amplitude and shape of the daily cloud cycle remain similar for horizontal res-
 103 olutions varying between 150 m and 2.5 km in ICON simulations. This setup allows us
 104 to directly access how an SST anomaly influences convection, to study possible interac-
 105 tions between clouds and DWLs in a highly realistic context, and to analyse global im-
 106 plications of including DWLs into models.

107 The main prerequisite for resolving DWLs in ocean simulations is high vertical res-
 108 olution of the upper oceanic layers (cf. Brilouet et al. (2021)). The introduction of the
 109 z^* ocean coordinate into the ICON model (detailed in Singh and Korn (in preparation))
 110 allows running global experiments with an unprecedented vertical resolution. For the pur-

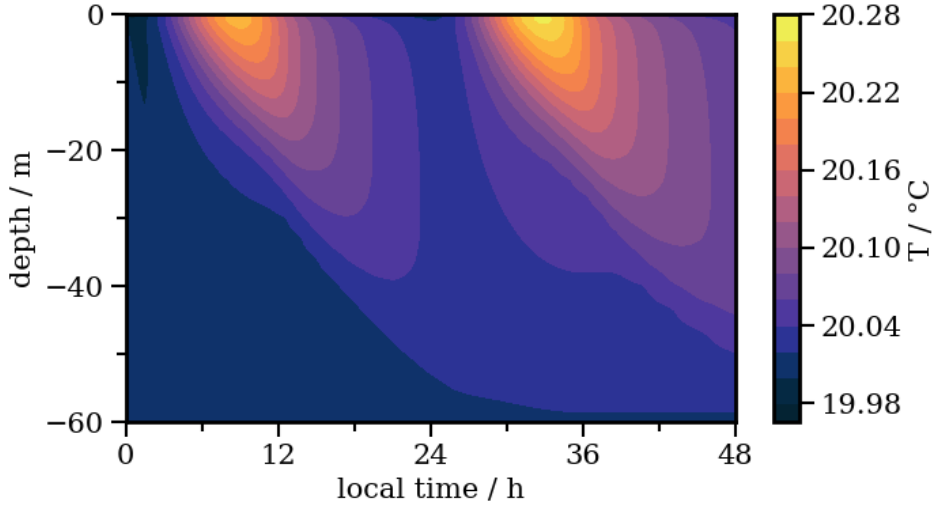


Figure 1: 48h simulation of DWLs in GOTM with the resolution specified in Figure A1 for an idealised heatflux with a maximal radiation of 600 W m^{-2} , a constant wind speed of 8 m s^{-1} , and a time step of 80 s.

111 poses of this article, we conducted two simulations. One has 128 ocean vertical levels,
 112 starting at 2 m at the surface and gradually growing with depth, which is also the setup
 113 in `G_A0_5km` in Hohenegger et al. (2022). This simulation plays the role of the reference
 114 simulation. The other has 139 ocean vertical levels, starting with 0.5 m and gradually
 115 increasing and blending into the reference setup from 45.4 m depth (see Figure A1 in
 116 the Appendix). To determine layer thicknesses necessary for resolving DWLs, while keep-
 117 ing the total number of layers as low as possible, we ran test simulations with the one
 118 dimensional ocean model GOTM (Umlauf et al. (2005)). The vertical grid that we chose
 119 is sufficiently coarse to obtain a numerically stable global run and produces DWLs whose
 120 temperature field is indistinguishable in its depth, magnitude and overall vertical struc-
 121 ture from a run with a 10 cm uniform grid (see Figure A2 in the Appendix and Figure
 122 1). We run both simulations for 30 days starting January 21 2020 and with the coupling
 123 and radiation time steps of 12 min, the atmosphere time step of 30 s, and the ocean time
 124 step of 80 s. Both simulations have identical initial conditions, whereby the generation
 125 of the initial ocean state is described in Hohenegger et al. (2022). We call the runs with
 126 128 and 139 ocean levels S_{control} and $S_{+\text{DWL}}$ respectively.

127 3 Representation of diurnal warm layers

128 In this section we describe the features of DWLs as represented in our simulations
 129 and compare them to known properties derived from measurements, reanalysis, and limited-
 130 area decameter-scale simulations. As our main focus is on tropical convection, we con-
 131 centrate our analysis on the tropics which we define here as the area comprised between
 132 40°N and 40°S .

133 3.1 Occurrence and magnitude

134 First we diagnose DWLs and assess their occurrence and magnitude. Rigorously
 135 speaking, DWLs are defined via vertical temperature gradients (see e.g. Matthews et al.
 136 (2014)), as they represent a temperature anomaly sitting on top of the ocean mixed layer.
 137 Instead of the temperature gradient, the daily SST amplitude (DSA) is often used as a

138 proxy (e.g. in Voltaire et al. (2022)), because, as mentioned in Bellenger and Duvel (2009),
 139 in the tropics one can assume that horizontal advection happens at longer time scales,
 140 and the temperature changes in the upper ocean can be attributed to DWLs. We also
 141 adopt this approach, formally defining DWLs as places with DSA larger than 0.1 K, which
 142 corresponds to non-zero depth of a DWL in Matthews et al. (2014). Care is required when
 143 following this approach, as SST in our model is defined as the temperature in the up-
 144 permost layer. In S_{+DWL} it is the average temperature over 0.5 m and in $S_{control}$ the av-
 145 erage temperature over 2 m. Since in this study our main interest is the response of the
 146 atmosphere, and since this is the temperature that the atmosphere sees, we do not cor-
 147 rect for this difference in our analysis.

148 In our simulations, DWLs are ubiquitous: Even spots with DSA of over 1.5 K cover
 149 5% of the tropical ocean area. Comparing DWLs in our simulations and in ERA5 reanal-
 150 ysis, we can see in Figure 2 that for the last 10 days of January the spatial distribution
 151 of DWLs is in good agreement with each other, with a correlation coefficient of 0.51. The
 152 major hot spots of DWLs are in the Indian ocean south of the equator, along the west-
 153 ern coasts of America and Africa, and in the southern part of the Pacific, both in our
 154 simulations and in ERA5. Similar areas are also identified in the January climatology
 155 map of Bellenger and Duvel (2009). A striking feature of our simulation is that, while
 156 for $S_{control}$ the DSA field appears nearly homogeneous and the extremes are underesti-
 157 mated compared to ERA5, as expected from the use of thick ocean vertical layers, the
 158 amplitudes in S_{+DWL} are much larger than in the reanalysis, with values twice as high.
 159 This is in contrast with observations summarised in Kawai and Wada (2007). Since Kawai
 160 and Wada (2007) employed the skin temperature to diagnose DWL, we can conclude that
 161 DSA is overestimated in S_{+DWL} . This is confirmed by further observations. The PIRATA
 162 buoys located at $0^{\circ}N10^{\circ}W$ and $0^{\circ}N0^{\circ}E$ at 1 m depth have each measured DSA of un-
 163 der 0.7 K in the same period, and the average DSA measured during the EUREC⁴A field
 164 campaign in the area $56.5^{\circ}W-59^{\circ}W$ and $12^{\circ}N-14.5^{\circ}N$ is about 0.15 K, while in S_{+DWL}
 165 the values at these locations are 1.8 K and 0.71 K respectively. A possible cause for the
 166 overestimation is insufficient vertical mixing in the upper layers of the ocean. As this study
 167 concentrates on the atmospheric effect of the DWLs, this problem does not jeopardise
 168 the analysis, and if anything indicates that the simulated effects will be too strong.

169 Another important feature is that in S_{+DWL} , DWLs tend to avoid areas with high
 170 cloud cover: on a given day, 24% of cells over the ocean have a cloud cover of 0.9 or higher,
 171 while for cells where DWLs develop this number reduces to 13%. However, there are also
 172 many areas with a low cloud cover and yet no significant DWLs, as shown in Figure 3.
 173 For instance, out of all areas with cloud cover below 0.3 on a given day, only 9% devel-
 174 oped DWLs with DSA of 1.5 K or higher. This is a consequence of a property well docu-
 175 mented in observational studies. Indeed, as explained in Soloviev and Lukas (2013), short-
 176 wave radiation and surface wind are the two principal driving factors of DWLs, where
 177 high shortwave radiation and low wind speed favor the appearance of DWLs. The pre-
 178 viously mentioned areas with low cloud cover but no DWL correspond to high-wind zones.
 179 The relationship of DWLs with downward shortwave radiation and near-surface wind
 180 speed will be further explored in Section 3.2.

181 As to the horizontal extent of DWLs as simulated by S_{+DWL} , there are two obser-
 182 vations to be made. As shown in Figure 4a, there are many small clusters of DWLs, but
 183 the total area they cover is practically negligible: although 177 clusters out of 799 are
 184 of size $\leq 625 \text{ km}^2$, the total area covered by them amounts to only 0.3% of the entire
 185 area covered by DWLs. On the opposite end of the histogram in Figure 4a, one can see
 186 that there are a few clusters of size 10^6 km^2 . They form predominantly in the high DSA
 187 areas from Figure 2 (not shown). Moreover, for each particular grid cell, the DWLs do
 188 not seem to be persistent: for instance, in a region with very high DSA in the Indian ocean
 189 (between $70^{\circ}E-75^{\circ}E$ and $5^{\circ}S-10^{\circ}S$, see the white square in Figure 2b) during a period
 190 of 30 days no episode of $DSA > 0.6 \text{ K}$ lasted longer than ten days, and 80% of all episodes

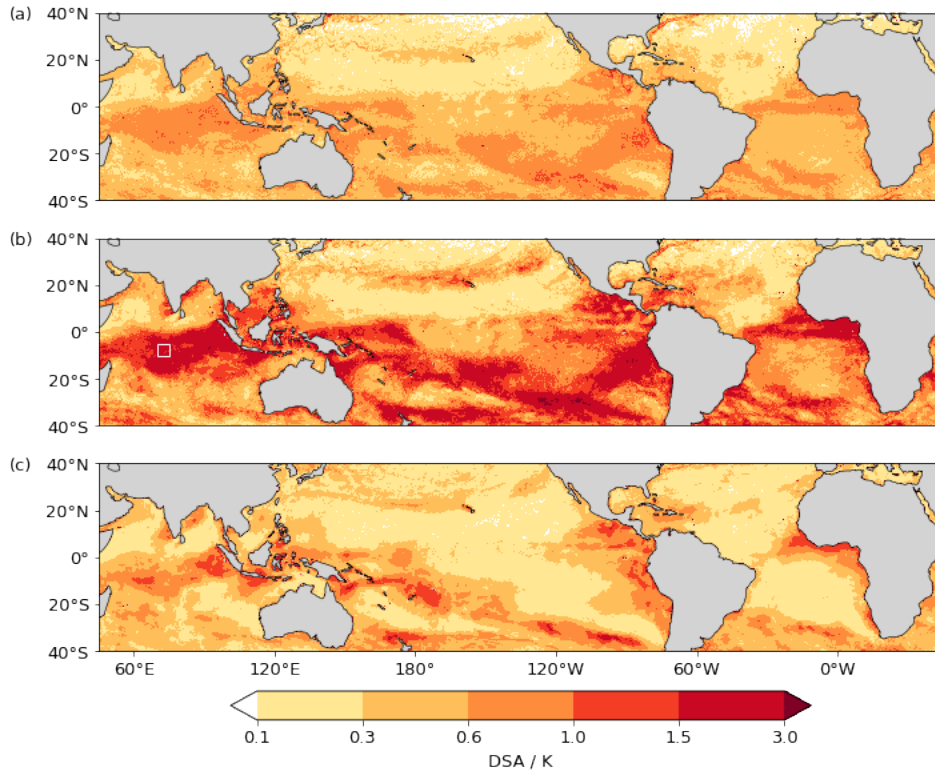


Figure 2: Magnitudes of the daily SST amplitude (max–min), averaged between 22 and 30 January 2020 in (a) S_{control} , (b) S_{+DWL} , and (c) ERA5. The white rectangle in (b) designates an area in the Indian ocean that is analysed in Section 3.1.

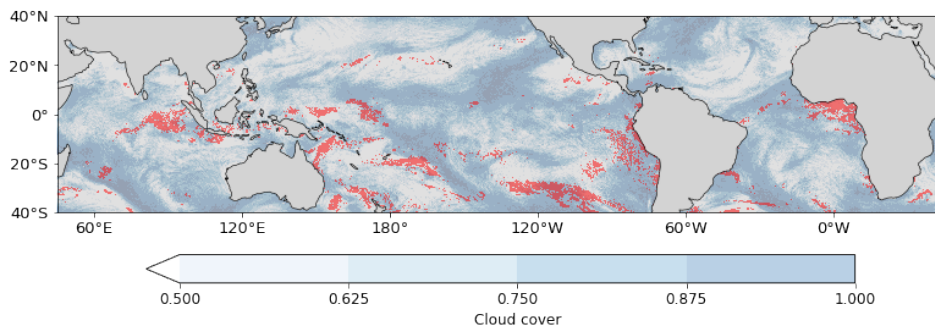


Figure 3: Cloud cover on a particular day (23 January 2020) in S_{+DWL} . Red areas correspond to DWL regions with DSA of over 1.5 K.

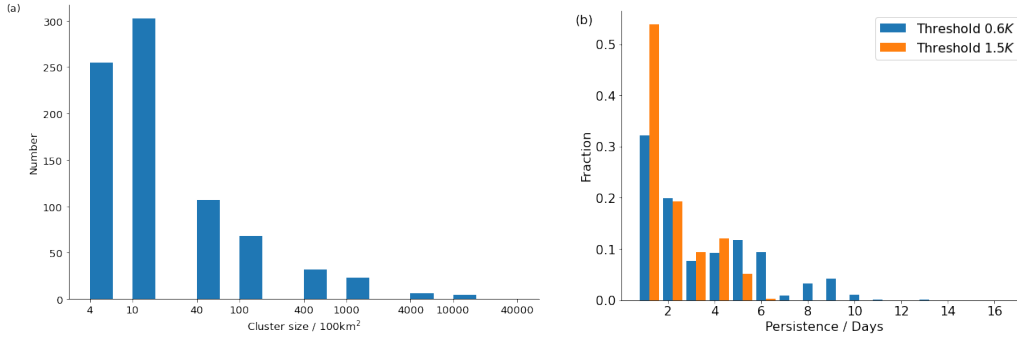


Figure 4: (a) Clusters of DWLs to the threshold of 1.5 K on a particular day (23 January 2020) ordered in a histogram of cluster sizes. (b) Normalised histogram of DWL episode lengths to different thresholds for the box 70°E–75° E and 5°S–10°S

191 lasted five days or less (see Figure 4b). Expectedly, the persistence time becomes shorter
 192 if a higher threshold for DSA is considered. This result is similar to the findings in the
 193 ERA40 forced simulation in Bellenger and Duvel (2009), where they showed that the DWL
 194 episode duration decays faster than exponentially.

195 **3.2 Structure of DWLs and preconditions for their formation**

196 For a deeper understanding of how the known properties of DWLs are captured
 197 by S_{+DWL} we focus on a study of this phenomenon in the tropical northern Atlantic re-
 198 gion off the coast of Barbados, more precisely in the box 56.5°W–59°W and 12°N–14.5°N
 199 corresponding to the region of the EUREC⁴A field campaign (Stevens et al. (2021)).

200 First, we examine the vertical structure of a DWL produced in the simulation S_{+DWL} .
 201 As shown in the anomaly profile (Figure 5), the incoming heat quickly accumulates in
 202 the upper layers during the day, as the warming of the upper layers creates a stable strat-
 203 ification if the mixing is slow, which is the case under low wind conditions. During the
 204 night, the DWL slowly dissipates until a single mixed layer is restored. As mentioned
 205 before, in this region, the heat anomalies are overestimated: a typical DSA in glider ob-
 206 servations is approximately 0.15 K (see Hohenegger et al. (2022), Figure 11c), while in
 207 S_{+DWL} in a calm period it is around 0.3 K. The time of the maximum and minimum is
 208 captured accurately compared to these observations (about 16 h LT and 8 h LT respec-
 209 tively).

Another analysis demonstrates that the dependency of DSA on insolation and sur-
 face wind observed, among others, in satellite measurements in Gentemann et al. (2003),
 are reproduced in ICON simulations as expected, namely higher DSA correlates with lower
 winds and higher downward shortwave radiation at the surface. The scatterplot in Fig-
 ure 6a shows a relationship similar to the formula

$$DSA \sim \begin{cases} U^{-3} & \text{for } U < 4\text{-}5 \text{ m s}^{-1}, \\ U^{-1} & \text{for } U > 4\text{-}5 \text{ m s}^{-1}, \end{cases}$$

210 suggested in Soloviev and Lukas (2013) for 10 m wind speed U , although the threshold
 211 appears to be located at 6–7 m s⁻¹ rather than at 4–5 m s⁻¹. Also the linear depen-
 212 dence on shortwave radiation described in Matthews et al. (2014) seems to be confirmed
 213 in S_{+DWL} (Figure 6b). In particular, the slope of the linear regression between DSA and
 214 surface downward shortwave radiation in ICON is 0.0023 K W⁻¹m², which is indeed close

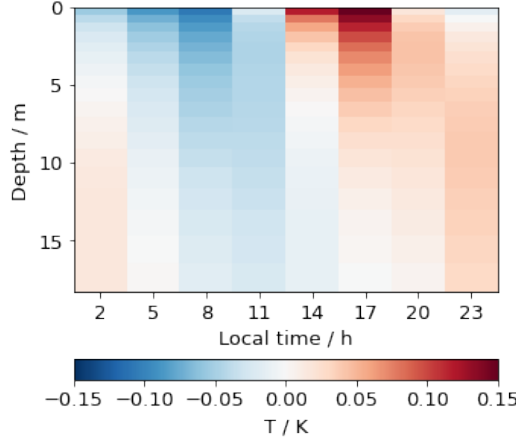


Figure 5: Sea water temperature (3 h output) averaged over 3 days over the box $56.5^{\circ}W$ - $59^{\circ}W$ and $12^{\circ}N$ - $14.5^{\circ}N$, time anomaly.

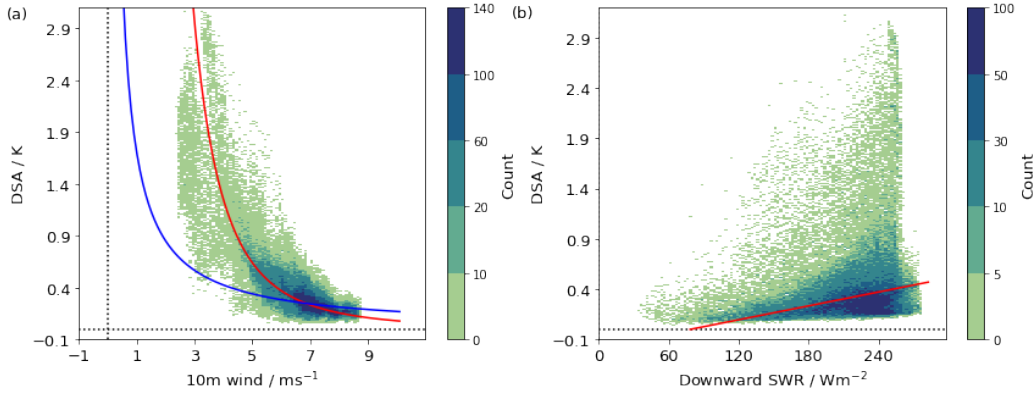


Figure 6: 2D histograms of SST amplitude and (a) 10 m wind speed as well as (b) short-wave radiation over the box $56.5^{\circ}W$ to $59^{\circ}W$ and $12^{\circ}N$ to $14.5^{\circ}N$ in S_{+DWL} . The blue and red lines in (a) indicate the interpolation of U^{-1} and U^{-3} to higher and lower wind speeds respectively. The red line in (b) is the linear regression fit between the variables.

215 to the slope of $0.0021 \text{ K W}^{-1}\text{m}^2$ found in Matthews et al. (2014). The large scattering
 216 of points in Figure 6b is caused by the joint influence of wind speed and radiation on DWLs.

217 **4 Effect of DWLs on convection**

218 The previous section shows that DWLs are frequent in the tropics, they cover large
 219 areas and persist over several days. We can therefore hypothesize that they might have
 220 an effect on atmospheric convection, either by creating horizontal air temperature gra-
 221 dents, or by enhancing the moistening of the overlying air. Moreover, as DSA in S_{+DWL}
 222 is overestimated, the effect of DWLs is expected to be too strong.

223 To assess the impact of DWLs on convective clouds, we need to compare the val-
 224 ues of relevant variables in places where DWLs develop to places where they do not devel-
 225 op. A clean way to accomplish this without having to account for other sources of vari-
 226 ability is to compare the differences between these values in S_{+DWL} and S_{control} at places

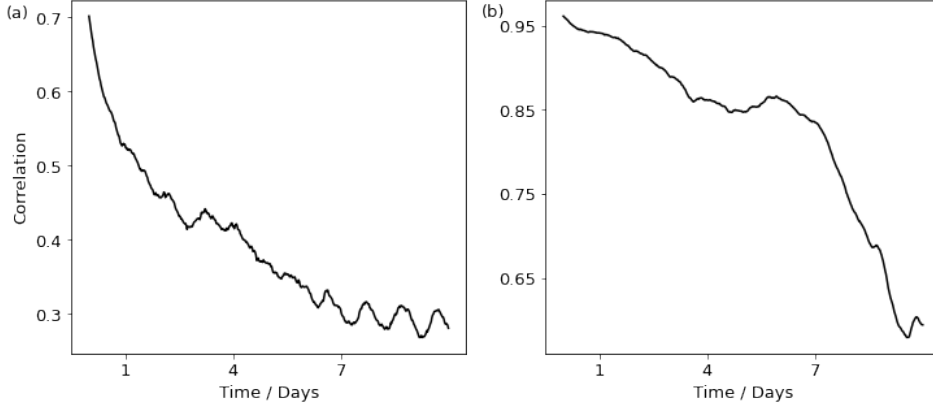


Figure 7: Temporal evolution of the global correlation between S_{control} and $S_{+\text{DWL}}$ for (a) cloud cover and (b) latent heat flux.

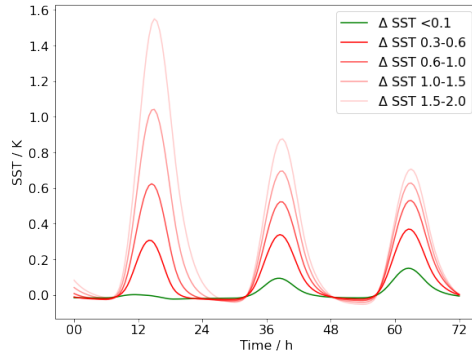


Figure 8: Time series (in local time) of $S_{+\text{DWL}} - S_{\text{control}}$ for different ΔSST .

227 where DWLs of a certain magnitude are present in $S_{+\text{DWL}}$. A key point in this analy-
 228 sis is to only include the first 4 days after the start of the simulation into the investiga-
 229 tion to ensure that the two simulations remain close and do not diverge due to the chaotic
 230 nature of the atmosphere. Figure 7 shows that both simulations indeed remain highly
 231 correlated during the first several days.

232 To conduct our analysis, we proceed as follows. The ocean is subdivided into $0.25^\circ \times$
 233 0.25° disjoint squares, and for each square the hourly maximal SST difference between
 234 $S_{+\text{DWL}}$ and S_{control} during a day, denoted by ΔSST , is computed. Based on this first day
 235 of the analysis that we also call the detection day, two groups can be formed: one called
 236 the "no DWL difference" group, where ΔSST stays below 0.1 K, and another one where
 237 ΔSST lies between certain thresholds T_1 and T_2 , which we call the "DWL difference be-
 238 tween T_1 and T_2 " group. Note that the plot of ΔSST yields a map very similar to Fig-
 239 ure 2b (Figure B1 in the Appendix), and thus can be used as a proxy for identifying DWL
 240 areas. We use this proxy from now on to cover a larger variety of cases and to obtain
 241 a cleaner comparison.

242 The subsequent analysis consists in comparing the two groups to each other, focusing
 243 on the time series of the differences in relevant variables over the days 1-3, with
 244 day 1 being the detection day, see Figure 8 for an example of the differences in SST. Sta-
 245 tistically, it is supported by t-tests for equality of means for independent samples with

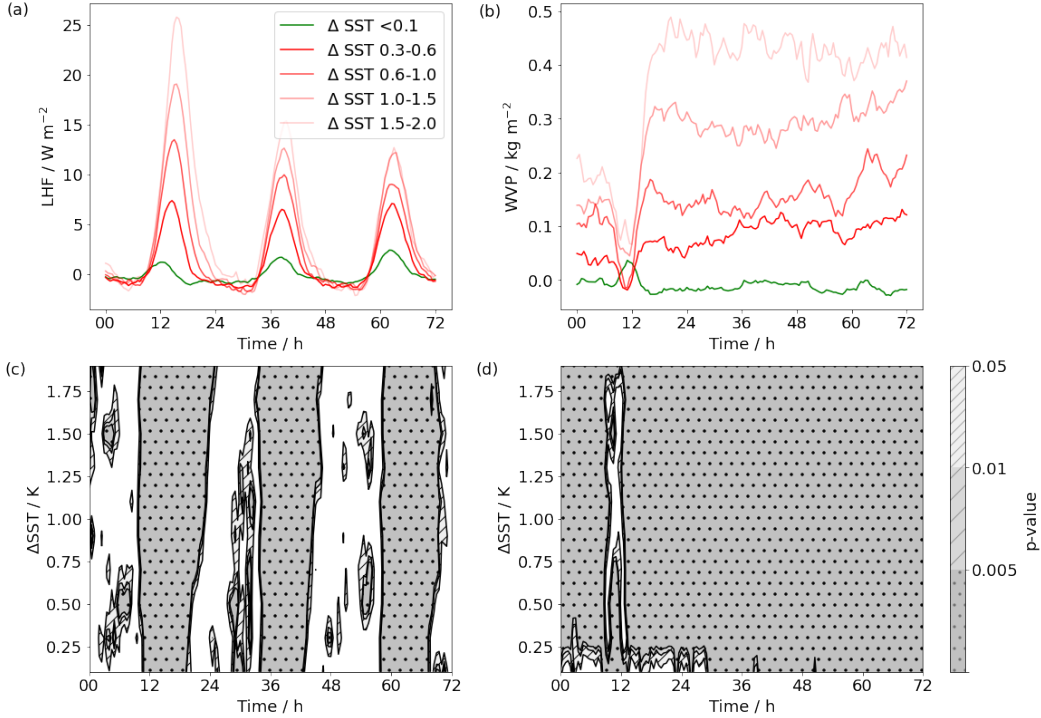


Figure 9: Time series (in local time) of $S_{+DWL}-S_{control}$ and t-test significance levels in bins of 0.1 K for LHF (a, c) and WVP (b, d). On panel c and d, white means not significant.

246 different variances. Every group with $T_2 - T_1 = 0.1$ K has at least 1695 cells, a suffi-
 247 cient number to ensure the robustness of the results. The size of the squares is chosen
 248 in accordance to the cluster sizes discussed in Section 3.1 (see Figure 4), as a mesoscale
 249 analysis is sufficient to capture a possible effect of DWLs, and also because the temper-
 250 ature and moisture changes produced by one isolated cell of $0.1^\circ \times 0.1^\circ$ are not expected
 251 to have a large effect and would be quickly mixed in the atmosphere. Moreover, we make
 252 the assumption that the effects in cloudiness are localised. Indeed, the impact of DWLs
 253 on cloud cover via moistening is a local effect, and the mesoscale circulation created by
 254 SST gradients would also result in cloud formation over DWLs. With this assumption,
 255 the samples can be treated as independent.

256 4.1 Impact on latent heat flux and related quantities

257 First we investigate whether higher ΔSST leads to more moisture in the air over
 258 DWL areas. This will help understand whether cloud formation may be impacted over
 259 DWLs. In particular, we are going to concentrate on differences in latent heat flux (LHF)
 260 and water vapor path (WVP) to measure the effects on evaporation and column moist-
 261 ening respectively, as shown in Figure 9.

262 The first observation concerning the plots (a, b) in Figure 9 is that the differences
 263 between S_{+DWL} and $S_{control}$ in the "no DWL difference" group after the detection day
 264 revolve around zero, as expected and further justifying our approach. This is not the case
 265 for the "DWL" groups. Differences are clearly appearing and are of larger magnitude,
 266 the stronger the DWL is.

267 The latent heat flux is increased when DWLs are present, with a peak around noon
 268 on every day, as expected from the daily cycle in SST. WVP is always higher over DWLs.
 269 The difference decreases in the morning hours of the detection day and increases rapidly
 270 thereafter. The dip could be caused either by a dip in LHF, by an increase of precipi-
 271 tation or by a weakening in convergence of moisture. As LHF is increased and there is
 272 no excessive rain over DWLs (not shown), the dip must be due to weaker convergence,
 273 which might be caused by a weakening of surface wind required for DWL formation. The
 274 increase of WVP after 12 h LT reflects the increase in moisture due to increased LHF.
 275 One can trace the propagation of the moisture response to DWLs in Figure 9, since the
 276 onset and duration times of the effects are different: while LHF reacts immediately and
 277 is tied directly to differences in temperature (see Figure 8), the effect on WVP is delayed
 278 by several hours and persists over the following days without losing its magnitude.

279 Figure 9(c, d) confirms that the differences observed visually are highly significant
 280 even on the third day and even for small Δ SST with p-values smaller than 0.005, except
 281 for the nighttime values of LHF. However, an important point is that the absolute dif-
 282 ferences are rather small, especially for smaller Δ SST: For instance, for Δ SST between
 283 0.6 K and 1.0 K, the peak of LHF is below 15 W m^{-2} and WVP is below 0.2 kg m^{-2} .
 284 One can compare these values with global averages of the two quantities over the ocean,
 285 which are ca. 130 W m^{-2} for LHF and ca. 34.6 kg m^{-2} for WVP. The order of magni-
 286 tude of LHF changes is similar to that found in the single column configuration in Voltaire
 287 et al. (2022).

288 4.2 Impact on cloudiness

289 The variables we consider for analysing the impact of DWLs on clouds are cloud
 290 cover (CC) and cloud liquid water (CLW).

291 The responses of CC and CLW shown in Figure 10 are very similar to each other.
 292 The "no DWL difference" time series is fluctuating around zero after the detection day,
 293 but on the detection day itself there is a peak at midday. In contrast, the DWLs regions
 294 exhibit dips at the same time, and the magnitude of these dips is positively correlated
 295 with the Δ SST amplitude (see Figure 10(a, b) and Figure 10(e, f)). This illustrates the
 296 prerequisite for DWLs to exist mentioned in Section 3.1: The appearance of DWLs is
 297 generally favored by a lower cloud amount. Subsequently we can observe the cloud re-
 298 sponse to the formation of DWLs on the detection day: after about 12 h LT, the differ-
 299 ence between S_{+DWL} and $S_{control}$ in both CC and CLW over DWLs starts to grow, and
 300 by 15 h LT both simulations have the same cloud amount. This growth is statistically
 301 significant starting from an SST amplitude of 0.3 K, and the effect persists longer for
 302 higher values of Δ SST, namely until 20 h LT for Δ SST of 1.5-2.0 K and until 18 h LT
 303 for Δ SST of 0.3-1.0 K for CC. Moreover, the effect seems to last longer for CLW, although
 304 the values of both variables fall back below the zero line already during the night. In to-
 305 tal, the increase of cloud following the formation of a DWL lasts up to 5-6 h.

306 A behaviour similar to the first day, that is, less CC and CLW in S_{+DWL} compared
 307 to $S_{control}$ in the morning and rise of these quantities in S_{+DWL} in the afternoon, can be
 308 observed also on the second and third day after the detection day (Figure 10(a, b)), how-
 309 ever, the deviation is barely significant: most of the time, the p-value is above 0.05, es-
 310 pecially for higher values of Δ SST (Figure 10(c, d)). This means that the increase of the
 311 quantities is often not homogeneous enough to be interpreted as systematic (see Figure
 312 10(c, d)). A crucial factor here is the absolute magnitude of the differences: In extreme
 313 cases, for Δ SST between 1.5 and 2.0 K, the deviation of CC reaches 0.03 and that of CLW
 314 0.02 kg m^{-2} on the detection day. On the following day the corresponding maximal val-
 315 ues fall to 0.01 and 0.01 kg m^{-2} , while the averages are 0.001 and 0.002 kg m^{-2} respec-
 316 tively (see Figure 10(a, b)). We can compare those to the average values of CC and CLW
 317 over DWLs, 0.65 for CC and 0.11 kg m^{-2} for CLW. The average increase in CLW is about

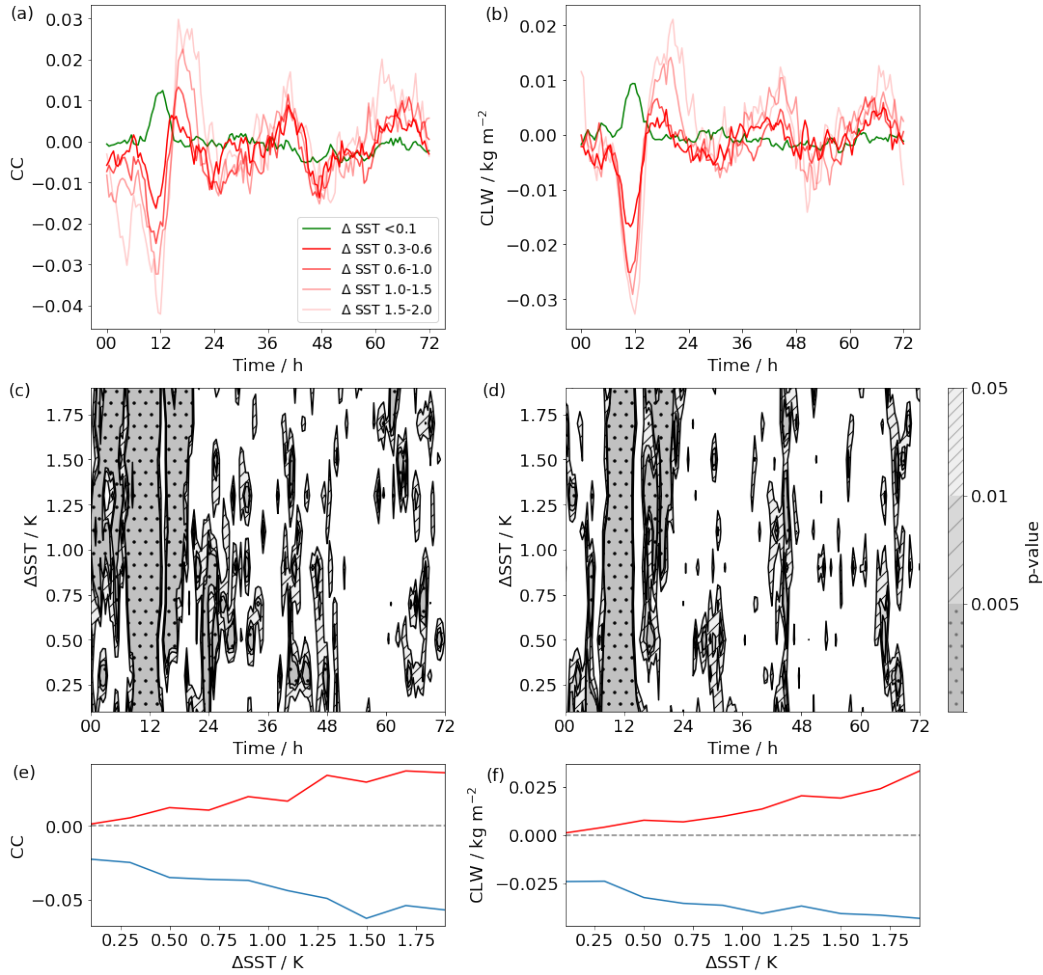


Figure 10: Time series (in local time) of $S_{+DWL} - S_{control}$, t-test significance levels in bins of 0.1 K, and maximal (red) and minimal (blue) value of the deviation on the detection day for CC (a, c, e) and CLW (b, d, f).

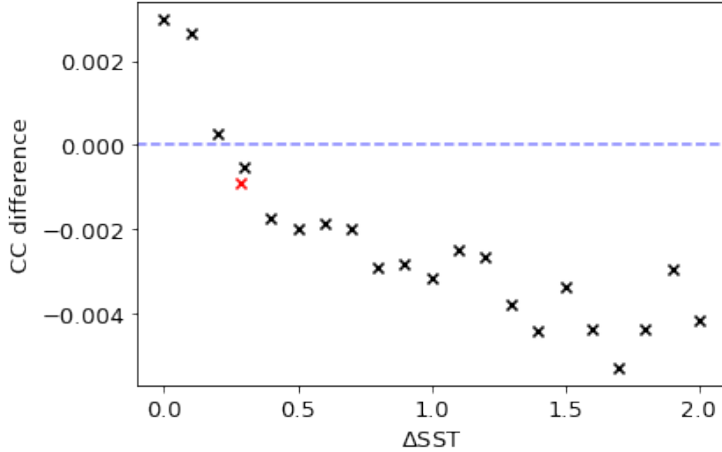


Figure 11: Daily mean CC differences ($S_{+DWL} - S_{control}$) as a function of ΔSST (black crosses). The red cross is the average CC difference against the average ΔSST .

318 1% and the increase in CC is about 0.2% on the day following even very large ΔSST .
 319 We can therefore conclude that the effect on the cloud water content is higher than the
 320 contribution of DWLs to cloud cover change, but the effects are very small.

321

322 The morning/midday dip of CC and CLW over DWLs even overcompensates the
 323 subsequent rise of these quantities. Figure 11 shows mean CC differences between S_{+DWL}
 324 and $S_{control}$ as a function of ΔSST on the detection day. For ΔSST above 0.3 K the sim-
 325 ulation S_{+DWL} has lower values of CC than $S_{control}$, and only for ΔSST below 0.3 K the
 326 reverse is true, such that on average, S_{+DWL} has slightly less cloud than $S_{control}$. The
 327 effect of DWLs appears to be dominated by the variability of the model. All in all, we
 328 can conclude that DWLs do not increase the global mean of cloud cover or cloud liquid
 329 water path.

330 We continue the analysis by looking at deep and shallower clouds separately, as one
 331 might expect to see more effects associated with one type of clouds. We differentiate be-
 332 tween deep and shallow clouds by taking the outgoing longwave radiation at the top of
 333 the atmosphere of 240 W m^{-2} as a threshold. This value is mentioned in Fu et al. (1990)
 334 as the threshold often used to identify deep convection. While the figures for shallower
 335 clouds are very similar to Figure 10 (not shown), the deviation for CLW in deep clouds
 336 is somewhat larger, up to 0.03 kg m^{-2} on the detection day. As shown in Figure 12a for
 337 CC, the effects, despite being a bit larger, remain very small and do not exhibit system-
 338 atic significance (Figure 12c). Considering precipitation as an additional possibility to
 339 see an impact of DWLs (Figure 12(b, d)), we see that there is no sufficient evidence to
 340 attribute the fluctuations of precipitation, even for higher values of ΔSST , to anything
 341 more than chance.

342 The last question that we want to investigate is to what extent the presence of DWLs
 343 might affect the diurnal cycle of convection. We focus on the example of the EUREC⁴A
 344 field campaign, which took place in the northern tropical Atlantic. For this region the
 345 diurnal cycle of shallow convection has been studied in great detail in Vial et al. (2019).
 346 In particular, it has been shown there that, in observations as well as in large-eddy sim-
 347 ulations (LES), the cloud cover peaks during the day, which might make it more suscep-
 348 tible to SST in comparison to other regions. In our case, both S_{+DWL} and $S_{control}$ over-

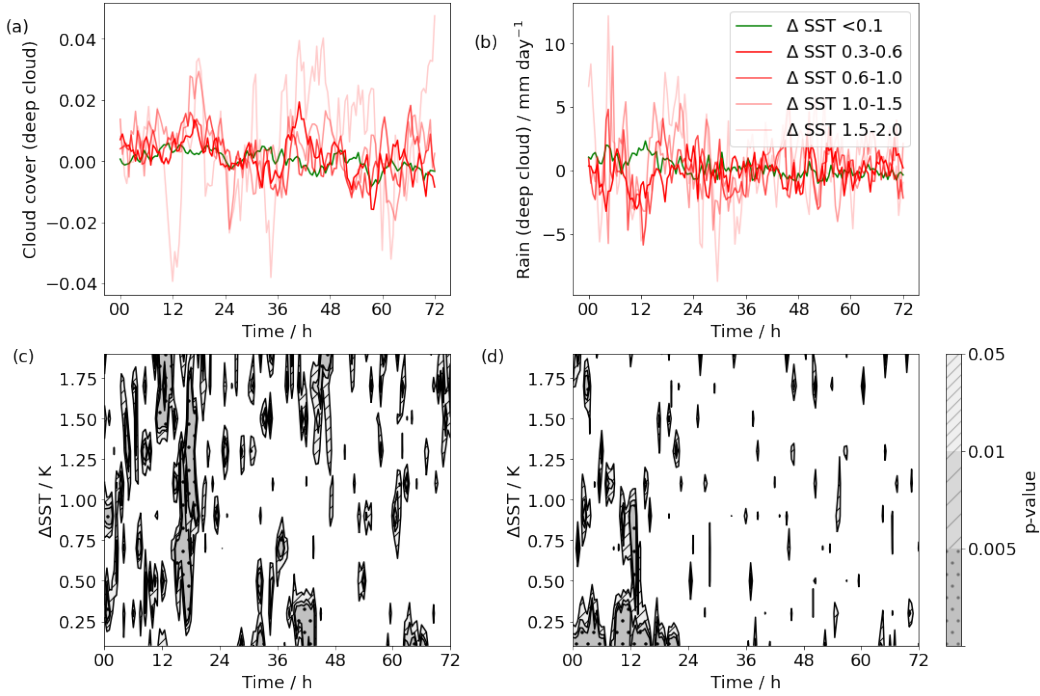


Figure 12: As Figure 9, but for CC (a, c) and precipitation (b, d) associated with deep convection.

349 estimate the CC found in observations by a factor of 2, as was expected from the res-
 350 olution sensitivity study in Vial et al. (2019), but capture perfectly the time structure
 351 as well as the amplitude of the cycle: minimum between 12 and 15 LT, maximum at 2
 352 LT, amplitude of about 0.1 (Figure 13), in good agreement with observations in Vial et
 353 al. (2019). The increase in CC resulting from the appearance of DWLs occurs in the late-
 354 afternoon. If anything, CC slightly decreases at other times. Both effects taken together
 355 tend to slightly reduce the diurnal amplitude. The fact that DWLs only have a small
 356 influence on the diurnal cycle of CC is consistent with the study in Vial et al. (2019) that
 357 reproduced the main features of the cycle in LES despite using fixed SST.

358 5 Discussion and conclusions

359 By introducing thin vertical levels into the global coupled ICON model, we could
 360 directly resolve diurnal warm layers (DWLs) and assess their impact on the atmosphere.
 361 The simulations employed a grid spacing of 5 km, both in the atmosphere and ocean,
 362 so that ocean mesoscale eddies and atmospheric convection can be resolved explicitly.
 363 The DWLs produced by the simulation reproduce the physical features known from ob-
 364 servations and limited area decameter simulations, but the magnitude of the daily SST
 365 fluctuations is exaggerated in comparison to reanalysis, by about a factor of two.

366 The increase in the amplitude of the diurnal cycle of SST in regions with diurnal
 367 warm layers leads to a corresponding increase in latent heat flux (LHF) and water va-
 368 por path (WVP). The effects are significant, even on days 2 and 3 following the detec-
 369 tion of a diurnal warm layer, but the values are small: 7 W m⁻² difference in LHF and
 370 0.1 kg m⁻² difference in WVP for a SST difference of 0.6 K. In the late-afternoon of the
 371 detection day, cloud cover (CC) and cloud liquid water (CLW) content also increase, but
 372 the effects are small and lose statistical significance within 5-6 hours of appearance. What

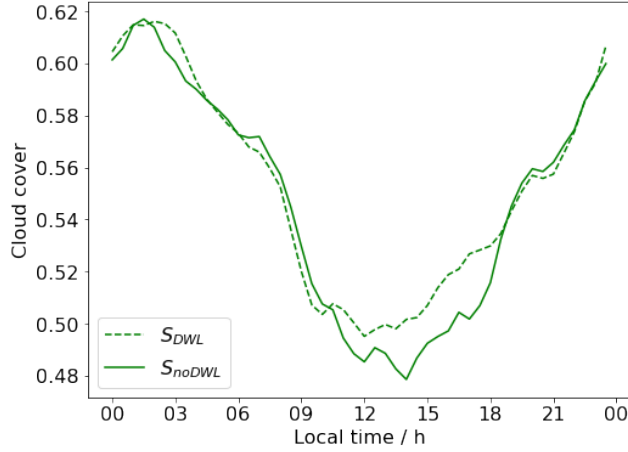


Figure 13: Diurnal cloud cover cycle in the box 56.5°W to 59°W and 12°N to 14.5°N, composite over 30 days.

373 is however significant is a decrease in cloud cover and liquid water content on the day
 374 of detection, around noon. This expresses the fact that diurnal warm layers favorably
 375 form in areas of low cloud cover, and hence high insolation. This effect compensates the
 376 subsequent increase. All in all, resolving diurnal warm layers does not affect the mean
 377 cloud cover over tropical oceans.

378 The amplitude of the observed differences in LHF is similar to findings in Voldoire
 379 et al. (2022), and the impact on cloud cover shows that convection over DWLs is enhanced,
 380 as it is claimed in the observation study of de Szoeke et al. (2021). Moreover, the small
 381 influence of DWLs on the CC cycle in the tropical Atlantic supports the results in Vial
 382 et al. (2019). A surprising and unprecedented finding of our study is the impact of DWLs
 383 on convection remains small even for a strongly enhanced daily SST amplitude over this
 384 particular region as well as globally.

385 We finish the discussion by focusing on the implications and limitations of our study.
 386 Regarding the question of the importance of DWLs in models, one needs to differenti-
 387 ate between the local and the overall impact. In our exemplary study in the northern
 388 tropical Atlantic, the presence of DWLs can reduce the amplitude of the diurnal cycle
 389 of the cloud cover by up to 10% (see Figure 13). In some specific cases with extraordi-
 390 narily high DSA, DWLs might indeed play a role. However, this remains a rare phenomenon.

391 The analysis in this manuscript only concerns short-term effects of DWLs. How-
 392 ever, it is known that the mean SST increases in DWL areas (Bellenger and Duvel (2009)).
 393 Therefore, inclusion of DWLs will have a long-term influence on the energy budget that
 394 is not treated here, but at least for short-term effects, our study demonstrates that DWLs
 395 do not have a global and significant impact.

396

Appendix A Vertical resolution of the simulations

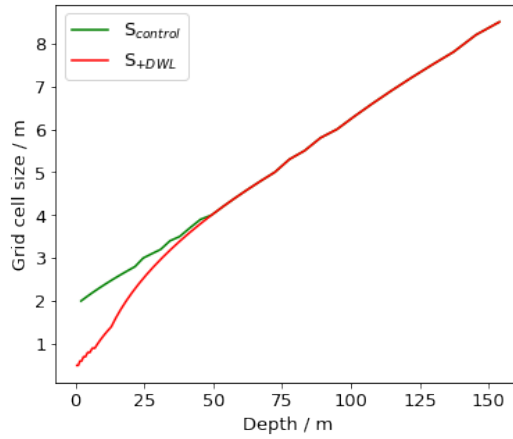


Figure A1: Layer thicknesses for S_{+DWL} and $S_{control}$

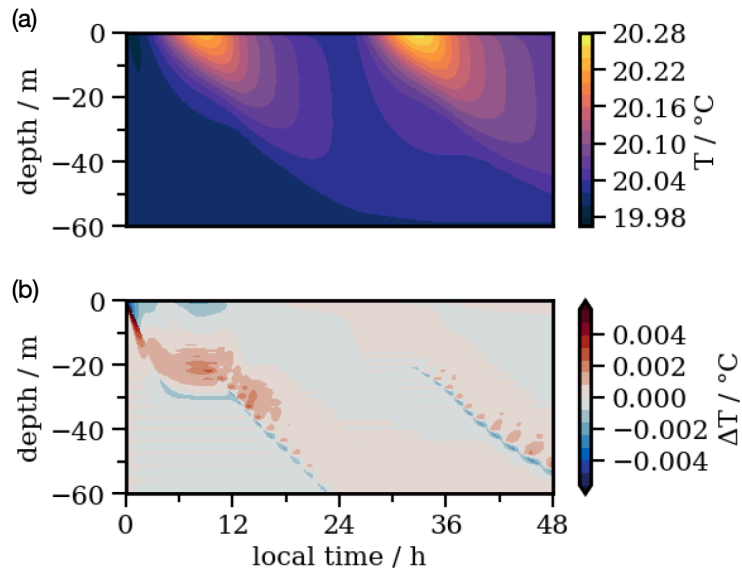
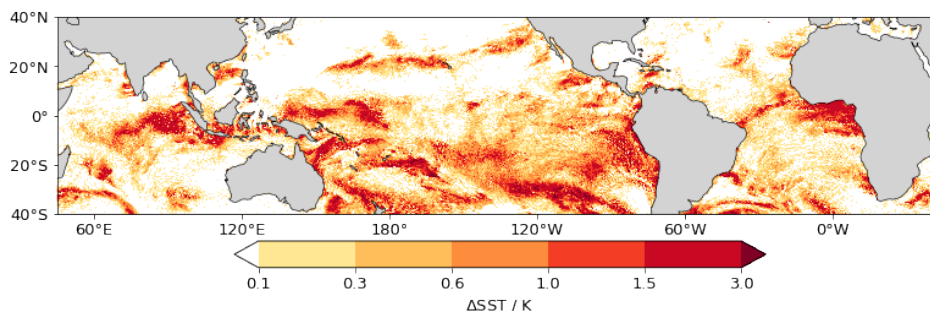


Figure A2: (a) As in Figure 1, but with uniform 0.1 m thick vertical layers. (b) Difference between the temperature profiles in Figure 1 and (a).

397

Appendix B Average ΔSST as proxy for DSA

Figure B1: Δ SST on detection day.

Appendix C Open Research

Detailed information concerning the ICON model is contained in the publication Hohenegger et al. (2022). The ocean model GOTM is documented in Umlauf et al. (2005) and can be installed from <https://gotm.net>. The ERA5 dataset used in this study has been provided by the Climate Data Store.

Acknowledgments

This work used resources of the Deutsches Klimarechenzentrum (DKRZ) granted by its Scientific Steering Committee (WLA) under project ID bm1253. The authors gratefully acknowledge the support of the DFG-funded collaborative research centre TRR181 "Energy Transfers in Atmosphere and Ocean".

References

- Bellenger, H., & Duvel, J.-P. (2009). An analysis of tropical ocean diurnal warm layers. *Journal of Climate*, *22*(13), 3629 - 3646. Retrieved from <https://journals.ametsoc.org/view/journals/clim/22/13/2008jcli2598.1.xml> doi: 10.1175/2008JCLI2598.1
- Brilouet, P.-E., Redelsperger, J.-L., Bouin, M.-N., Couvreur, F., & Lebeaupin Brossier, C. (2021). A case-study of the coupled ocean-atmosphere response to an oceanic diurnal warm layer. *Quarterly Journal of the Royal Meteorological Society*, *147*(736), 2008-2032. Retrieved from <https://rmets.onlinelibrary.wiley.com/doi/abs/10.1002/qj.4007> doi: <https://doi.org/10.1002/qj.4007>
- de Szoeko, S. P., Marke, T., & Brewer, W. A. (2021). Diurnal ocean surface warming drives convective turbulence and clouds in the atmosphere. *Geophysical Research Letters*, *48*(4), e2020GL091299. Retrieved from <https://agupubs.onlinelibrary.wiley.com/doi/abs/10.1029/2020GL091299> (e2020GL091299 2020GL091299) doi: <https://doi.org/10.1029/2020GL091299>
- Fu, R., Genio, A. D. D., & Rossow, W. B. (1990). Behavior of deep convective clouds in the tropical pacific deduced from isccp radiances. *Journal of Climate*, *3*(10), 1129 - 1152.
- Gentemann, C. L., Donlon, C. J., Stuart-Menteth, A., & Wentz, F. J. (2003). Diurnal signals in satellite sea surface temperature measurements. *Geophysical Research Letters*, *30*(3). Retrieved from <https://agupubs.onlinelibrary.wiley.com/doi/abs/10.1029/2002GL016291> doi: <https://doi.org/10.1029/2002GL016291>
- Hohenegger, C., Korn, P., Linardakis, L., Redler, R., Schnur, R., Adamidis, P.,

- 433 ... Stevens, B. (2022). Icon-sapphire: simulating the components of the
 434 earth system and their interactions at kilometer and subkilometer scales.
 435 *Geoscientific Model Development Discussions*, 2022, 1–42. Retrieved
 436 from <https://gmd.copernicus.org/preprints/gmd-2022-171/> doi:
 437 10.5194/gmd-2022-171
- 438 Hohenegger, C., Kornblueh, L., Klocke, D., Becker, T., Cioni, G., Engels, J. F., ...
 439 Stevens, B. (2020). Climate statistics in global simulations of the atmosphere,
 440 from 80 to 2.5 km grid spacing. *Journal of the Meteorological Society of Japan*.
 441 *Ser. II*, 98(1), 73-91. doi: 10.2151/jmsj.2020-005
- 442 Kawai, Y., & Wada, A. (2007). Diurnal sea surface temperature variation and
 443 its impact on the atmosphere and ocean: A review. *Journal of Oceanog-*
 444 *raphy*, 63(5), 721–744. Retrieved from [https://doi.org/10.1007/](https://doi.org/10.1007/s10872-007-0063-0)
 445 [s10872-007-0063-0](https://doi.org/10.1007/s10872-007-0063-0) doi: 10.1007/s10872-007-0063-0
- 446 Matthews, A. J., Baranowski, D. B., Heywood, K. J., Flatau, P. J., & Schmidtko,
 447 S. (2014). The surface diurnal warm layer in the indian ocean dur-
 448 ing cindy/dynamo. *Journal of Climate*, 27(24), 9101 - 9122. Retrieved
 449 from [https://journals.ametsoc.org/view/journals/clim/27/24/](https://journals.ametsoc.org/view/journals/clim/27/24/jcli-d-14-00222.1.xml)
 450 [jcli-d-14-00222.1.xml](https://journals.ametsoc.org/view/journals/clim/27/24/jcli-d-14-00222.1.xml) doi: 10.1175/JCLI-D-14-00222.1
- 451 Price, J. F., Weller, R. A., & Pinkel, R. (1986). Diurnal cycling: Observations
 452 and models of the upper ocean response to diurnal heating, cooling, and
 453 wind mixing. *Journal of Geophysical Research: Oceans*, 91(C7), 8411-8427.
 454 Retrieved from [https://agupubs.onlinelibrary.wiley.com/doi/abs/](https://agupubs.onlinelibrary.wiley.com/doi/abs/10.1029/JC091iC07p08411)
 455 [10.1029/JC091iC07p08411](https://doi.org/10.1029/JC091iC07p08411) doi: <https://doi.org/10.1029/JC091iC07p08411>
- 456 Soloviev, A., & Lukas, R. (2013). *The near-surface layer of the ocean: Structure, dy-*
 457 *namics and applications*. Springer Netherlands. Retrieved from [https://books](https://books.google.de/books?id=_4zHBAAAQBAJ)
 458 [.google.de/books?id=_4zHBAAAQBAJ](https://books.google.de/books?id=_4zHBAAAQBAJ)
- 459 Stevens, B., Bony, S., Farrell, D., Ament, F., Blyth, A., Fairall, C., ... Zöger,
 460 M. (2021). Eurec⁴a. *Earth System Science Data*, 13(8), 4067–4119. Re-
 461 trieved from <https://essd.copernicus.org/articles/13/4067/2021/> doi:
 462 10.5194/essd-13-4067-2021
- 463 Sverdrup, H., Johnson, M., & Fleming, R. (1942). *The oceans, their physics,*
 464 *chemistry, and general biology*. Prentice-Hall, Incorporated. Retrieved from
 465 <https://books.google.de/books?id=h74gAAAAMAAJ>
- 466 Umlauf, L., Bolding, K., & Burchard, H. (2005). *GOTM – scientific documentation,*
 467 *version 3.2* (Vol. 63). Leibniz-Institute for Baltic Sea Research, Warnemünde,
 468 Germany. Retrieved from <https://gotm.net/manual/stable/pdf/a4.pdf>
- 469 Vial, J., Vogel, R., Bony, S., Stevens, B., Winker, D. M., Cai, X., ... Brogniez,
 470 H. (2019). A new look at the daily cycle of trade wind cumuli. *Jour-*
 471 *nal of Advances in Modeling Earth Systems*, 11(10), 3148-3166. Retrieved
 472 from [https://agupubs.onlinelibrary.wiley.com/doi/abs/10.1029/](https://agupubs.onlinelibrary.wiley.com/doi/abs/10.1029/2019MS001746)
 473 [2019MS001746](https://doi.org/10.1029/2019MS001746) doi: <https://doi.org/10.1029/2019MS001746>
- 474 Voltaire, A., Roehrig, R., Giordani, H., Waldman, R., Zhang, Y., Xie, S., & Bouin,
 475 M.-N. (2022). Assessment of the sea surface temperature diurnal cycle in
 476 cnrm-cm6-1 based on its 1d coupled configuration. *Geoscientific Model Devel-*
 477 *opment*, 15(8), 3347–3370. Retrieved from [https://gmd.copernicus.org/](https://gmd.copernicus.org/articles/15/3347/2022/)
 478 [articles/15/3347/2022/](https://gmd.copernicus.org/articles/15/3347/2022/) doi: 10.5194/gmd-15-3347-2022
- 479 Wick, G. A., & Castro, S. L. (2020). Assessment of extreme diurnal warming in
 480 operational geosynchronous satellite sea surface temperature products. *Remote*
 481 *Sensing*, 12(22). Retrieved from [https://www.mdpi.com/2072-4292/12/22/](https://www.mdpi.com/2072-4292/12/22/3771)
 482 [3771](https://www.mdpi.com/2072-4292/12/22/3771) doi: 10.3390/rs12223771

1
2
3
4
5
6
7
8
9
10
11

Impact of Diurnal Warm Layers on Atmospheric Convection

Radomyra Shevchenko¹, Cathy Hohenegger¹, and Mira Schmitt²

¹Max Planck Institute for Meteorology, Hamburg, Germany
²Leibniz Institute for Baltic Sea Research, Warnemünde, Germany

Key Points:

- Diurnal warm layers increase atmospheric moisture.
- The increase of cloud cover following the formation of a diurnal warm layer is immediate and only lasts for several hours.
- The magnitude of the cloud cover increase is small and has no discernible influence on the global mean.

Corresponding author: Radomyra Shevchenko, radomyra.shevchenko@mpimet.mpg.de

Abstract

This manuscript presents a study of oceanic diurnal warm layers in kilometer-scale global coupled simulations and their impact on atmospheric convection in the tropics. With the implementation of thin vertical levels in the ocean, diurnal warm layers are directly resolved, and sea surface temperature (SST) fluctuations of up to several Kelvin appear in regions with low wind and high solar radiation. The increase of SST during the day causes an abrupt afternoon increase of atmospheric moisture due to enhanced latent heat flux, followed by an increase in cloud cover and cloud liquid water. However, although the daily SST amplitude is exaggerated in comparison to reanalysis, this effect only lasts for 5-6 hours and leads to an absolute difference of 1% for cloud cover and 0.01 kg m^{-2} for cloud liquid water. All in all, the impact of diurnal warm layers on convective cloud cover is found to be negligible in the tropical mean.

Plain Language Summary

The daily fluctuations of sea surface temperature (SST) have been extensively studied for the last decades, but the assessment of importance of this phenomenon for atmospheric convection on the global scale has come within reach only very recently, thanks to the development of simulations with a horizontal resolution of $O(1 \text{ km})$. In this manuscript we show that we can indeed observe an impact of SST fluctuations on moisture in the atmosphere. However, the impact on the amount of cloud in the tropics is found to be short-lived and its magnitude negligible on average.

1 Introduction

Diurnal sea surface temperature anomalies and their interplay with the atmosphere and in particular with the diurnal cycle of convection have been an object of study for many decades. In this study, we investigate this connection for the first time using simulations that can explicitly resolve both the daily temperature variations in the ocean and convection in the atmosphere on a global scale.

Daily variations in sea surface temperature (SST) have already been described in Sverdrup et al. (1942). Since then, there have been numerous studies describing the physics and the conditions of appearance of daily sea surface temperature (SST) variations, the seminal work by Price et al. (1986) being the first detailed description of this phenomenon. Under low-wind conditions and with sufficient insolation, a stable near-surface layer forms during the day in the upper layers of the ocean (until the depth of $O(10 \text{ m})$) that leads to a surface warming of up to 5 K (see Wick and Castro (2020)). In absence of solar radiation during the night, the stratification dissolves as vertical turbulent mixing takes overhand, until a homogeneous mixed layer is restored. The physics of this phenomenon is described in detail in a monograph by Soloviev and Lukas (2013). This stratified, warm layer is known as diurnal warm layer (DWL) and it is ubiquitous in all latitudes, causing SST fluctuations of 0.2 K or more in the entire Northern hemisphere and beyond during boreal summer (see Gentemann et al. (2003)). A comprehensive discussion of its definition and properties can be found in a review by Kawai and Wada (2007). In particular, the authors of the review point out that the presence of DWLs in observations as well as in single column simulations leads to stronger latent and sensible heat fluxes. As surface fluxes connect the surface to the atmospheric boundary layer and since changes in boundary layer properties affect the development of convection, the question of the impacts of DWLs on atmospheric convection arises.

Investigating this question in models requires both fine enough vertical resolution in the ocean, to resolve DWLs, and fine enough horizontal grid spacing in the atmosphere, to resolve atmospheric convection. With the development of deca- to kilometer scale simulations in a coupled configuration such investigations are becoming possible. Prominent

61 among the newest studies are the papers by Voldoire et al. (2022) and Brilouet et al. (2021).
 62 In Voldoire et al. (2022), a single column coupled model has been considered, while in
 63 Brilouet et al. (2021), a one column ocean model has been coupled to an atmospheric
 64 large-eddy simulation model integrated over a limited area. Both experiments are based
 65 on or validated with the data from the Dynamics of the Madden Julian Oscillation (DY-
 66 NAMO) campaign, during which daily SST differences of several Kelvin were observed.
 67 Voldoire et al. (2022) showed that the impact of DWLs on the boundary layer depth,
 68 atmospheric moisture and precipitation seems to be small. In contrast, de Szoeke et al.
 69 (2021) argued that in the observations from the DYNAMO data set, convection is en-
 70 hanced on days with large SST differences. Finally, Voldoire et al. (2022) conjectured
 71 that a single column model cannot capture horizontal interactions that might lead to a
 72 larger impact.

73 To the authors' knowledge, there is yet no study extending the question of inter-
 74 actions between DWLs and atmospheric convection to a realistic, global framework with
 75 resolved convection. And yet, atmospheric convection plays a key role in the energy and
 76 water cycle in the tropics, therefore describing the driving mechanisms of convection and
 77 assessing their importance is crucial.

78 The present study aims at closing this gap and precisely analysing the impact of
 79 DWLs on atmospheric convection in a global, coupled ICON simulation with 5km hor-
 80 izontal resolution and decameter grid spacing in the first oceanic layers. This allows us
 81 to resolve DWL and convection, to assess their interactions, also by resolving horizon-
 82 tal gradients, and to analyse the global impacts of DWLs. We are particularly interested
 83 in understanding whether the presence of DWLs enhances cloud cover in a time frame
 84 of several days and if so, whether this happens through a direct moistening by the la-
 85 tent heat flux or by enhancing spatial gradient in SST and mesoscale circulations. More-
 86 over, the global nature of our simulation allows to zoom in on different areas and encom-
 87 pass other meteorological and sea conditions than the ones of the DYNAMO campaign.

88 The manuscript is structured as follows. In Section 2 we describe the setup of the
 89 experiments, and in Section 3 we analyse the representation and properties of DWLs in
 90 global ICON simulations. In Section 4 we quantify the effect of DWLs on surface fluxes,
 91 atmospheric moisture and clouds, and finally in Section 5 we present the conclusions of
 92 our work.

93 2 Experimental setup

94 To study the effect of DWLs, we conduct global coupled simulations with the ICON
 95 model in its Sapphire configuration. The Sapphire configuration targets simulations with
 96 a horizontal grid spacing finer than 10 km. For our simulations, we use a setup similar
 97 to the simulation called `G_A0_5km` in Hohenegger et al. (2022), with small deviations that
 98 will be described below. The model is fully coupled, and at the horizontal resolution of
 99 approximately 5 km it is at the boundary of resolving convection. Although the cloud
 100 amount associated with shallow convection is expected to be overestimated (see Vial et
 101 al. (2019) and Hohenegger et al. (2020)), it has been demonstrated in Vial et al. (2019)
 102 that both amplitude and shape of the daily cloud cycle remain similar for horizontal res-
 103 olutions varying between 150 m and 2.5 km in ICON simulations. This setup allows us
 104 to directly access how an SST anomaly influences convection, to study possible interac-
 105 tions between clouds and DWLs in a highly realistic context, and to analyse global im-
 106 plications of including DWLs into models.

107 The main prerequisite for resolving DWLs in ocean simulations is high vertical res-
 108 olution of the upper oceanic layers (cf. Brilouet et al. (2021)). The introduction of the
 109 z^* ocean coordinate into the ICON model (detailed in Singh and Korn (in preparation))
 110 allows running global experiments with an unprecedented vertical resolution. For the pur-

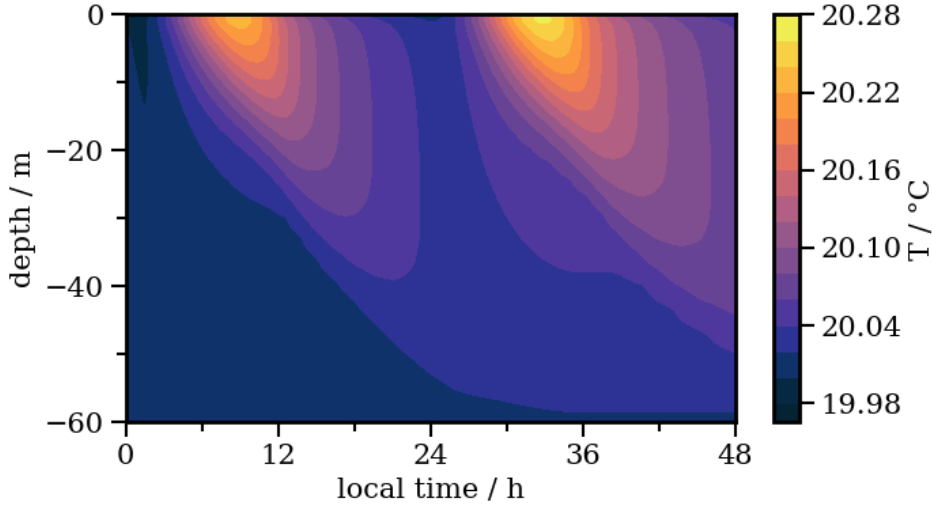


Figure 1: 48h simulation of DWLs in GOTM with the resolution specified in Figure A1 for an idealised heatflux with a maximal radiation of 600 W m^{-2} , a constant wind speed of 8 m s^{-1} , and a time step of 80 s.

111 poses of this article, we conducted two simulations. One has 128 ocean vertical levels,
 112 starting at 2 m at the surface and gradually growing with depth, which is also the setup
 113 in `G_A0_5km` in Hohenegger et al. (2022). This simulation plays the role of the reference
 114 simulation. The other has 139 ocean vertical levels, starting with 0.5 m and gradually
 115 increasing and blending into the reference setup from 45.4 m depth (see Figure A1 in
 116 the Appendix). To determine layer thicknesses necessary for resolving DWLs, while keep-
 117 ing the total number of layers as low as possible, we ran test simulations with the one
 118 dimensional ocean model GOTM (Umlauf et al. (2005)). The vertical grid that we chose
 119 is sufficiently coarse to obtain a numerically stable global run and produces DWLs whose
 120 temperature field is indistinguishable in its depth, magnitude and overall vertical struc-
 121 ture from a run with a 10 cm uniform grid (see Figure A2 in the Appendix and Figure
 122 1). We run both simulations for 30 days starting January 21 2020 and with the coupling
 123 and radiation time steps of 12 min, the atmosphere time step of 30 s, and the ocean time
 124 step of 80 s. Both simulations have identical initial conditions, whereby the generation
 125 of the initial ocean state is described in Hohenegger et al. (2022). We call the runs with
 126 128 and 139 ocean levels S_{control} and $S_{+\text{DWL}}$ respectively.

127 3 Representation of diurnal warm layers

128 In this section we describe the features of DWLs as represented in our simulations
 129 and compare them to known properties derived from measurements, reanalysis, and limited-
 130 area decameter-scale simulations. As our main focus is on tropical convection, we con-
 131 centrate our analysis on the tropics which we define here as the area comprised between
 132 40°N and 40°S .

133 3.1 Occurrence and magnitude

134 First we diagnose DWLs and assess their occurrence and magnitude. Rigorously
 135 speaking, DWLs are defined via vertical temperature gradients (see e.g. Matthews et al.
 136 (2014)), as they represent a temperature anomaly sitting on top of the ocean mixed layer.
 137 Instead of the temperature gradient, the daily SST amplitude (DSA) is often used as a

138 proxy (e.g. in Voltaire et al. (2022)), because, as mentioned in Bellenger and Duvel (2009),
 139 in the tropics one can assume that horizontal advection happens at longer time scales,
 140 and the temperature changes in the upper ocean can be attributed to DWLs. We also
 141 adopt this approach, formally defining DWLs as places with DSA larger than 0.1 K, which
 142 corresponds to non-zero depth of a DWL in Matthews et al. (2014). Care is required when
 143 following this approach, as SST in our model is defined as the temperature in the up-
 144 permost layer. In S_{+DWL} it is the average temperature over 0.5 m and in $S_{control}$ the av-
 145 erage temperature over 2 m. Since in this study our main interest is the response of the
 146 atmosphere, and since this is the temperature that the atmosphere sees, we do not cor-
 147 rect for this difference in our analysis.

148 In our simulations, DWLs are ubiquitous: Even spots with DSA of over 1.5 K cover
 149 5% of the tropical ocean area. Comparing DWLs in our simulations and in ERA5 reanal-
 150 ysis, we can see in Figure 2 that for the last 10 days of January the spatial distribution
 151 of DWLs is in good agreement with each other, with a correlation coefficient of 0.51. The
 152 major hot spots of DWLs are in the Indian ocean south of the equator, along the west-
 153 ern coasts of America and Africa, and in the southern part of the Pacific, both in our
 154 simulations and in ERA5. Similar areas are also identified in the January climatology
 155 map of Bellenger and Duvel (2009). A striking feature of our simulation is that, while
 156 for $S_{control}$ the DSA field appears nearly homogeneous and the extremes are underesti-
 157 mated compared to ERA5, as expected from the use of thick ocean vertical layers, the
 158 amplitudes in S_{+DWL} are much larger than in the reanalysis, with values twice as high.
 159 This is in contrast with observations summarised in Kawai and Wada (2007). Since Kawai
 160 and Wada (2007) employed the skin temperature to diagnose DWL, we can conclude that
 161 DSA is overestimated in S_{+DWL} . This is confirmed by further observations. The PIRATA
 162 buoys located at $0^{\circ}N10^{\circ}W$ and $0^{\circ}N0^{\circ}E$ at 1 m depth have each measured DSA of un-
 163 der 0.7 K in the same period, and the average DSA measured during the EUREC⁴A field
 164 campaign in the area $56.5^{\circ}W-59^{\circ}W$ and $12^{\circ}N-14.5^{\circ}N$ is about 0.15 K, while in S_{+DWL}
 165 the values at these locations are 1.8 K and 0.71 K respectively. A possible cause for the
 166 overestimation is insufficient vertical mixing in the upper layers of the ocean. As this study
 167 concentrates on the atmospheric effect of the DWLs, this problem does not jeopardise
 168 the analysis, and if anything indicates that the simulated effects will be too strong.

169 Another important feature is that in S_{+DWL} , DWLs tend to avoid areas with high
 170 cloud cover: on a given day, 24% of cells over the ocean have a cloud cover of 0.9 or higher,
 171 while for cells where DWLs develop this number reduces to 13%. However, there are also
 172 many areas with a low cloud cover and yet no significant DWLs, as shown in Figure 3.
 173 For instance, out of all areas with cloud cover below 0.3 on a given day, only 9% devel-
 174 oped DWLs with DSA of 1.5 K or higher. This is a consequence of a property well docu-
 175 mented in observational studies. Indeed, as explained in Soloviev and Lukas (2013), short-
 176 wave radiation and surface wind are the two principal driving factors of DWLs, where
 177 high shortwave radiation and low wind speed favor the appearance of DWLs. The pre-
 178 viously mentioned areas with low cloud cover but no DWL correspond to high-wind zones.
 179 The relationship of DWLs with downward shortwave radiation and near-surface wind
 180 speed will be further explored in Section 3.2.

181 As to the horizontal extent of DWLs as simulated by S_{+DWL} , there are two obser-
 182 vations to be made. As shown in Figure 4a, there are many small clusters of DWLs, but
 183 the total area they cover is practically negligible: although 177 clusters out of 799 are
 184 of size $\leq 625 \text{ km}^2$, the total area covered by them amounts to only 0.3% of the entire
 185 area covered by DWLs. On the opposite end of the histogram in Figure 4a, one can see
 186 that there are a few clusters of size 10^6 km^2 . They form predominantly in the high DSA
 187 areas from Figure 2 (not shown). Moreover, for each particular grid cell, the DWLs do
 188 not seem to be persistent: for instance, in a region with very high DSA in the Indian ocean
 189 (between $70^{\circ}E-75^{\circ}E$ and $5^{\circ}S-10^{\circ}S$, see the white square in Figure 2b) during a period
 190 of 30 days no episode of $DSA > 0.6 \text{ K}$ lasted longer than ten days, and 80% of all episodes

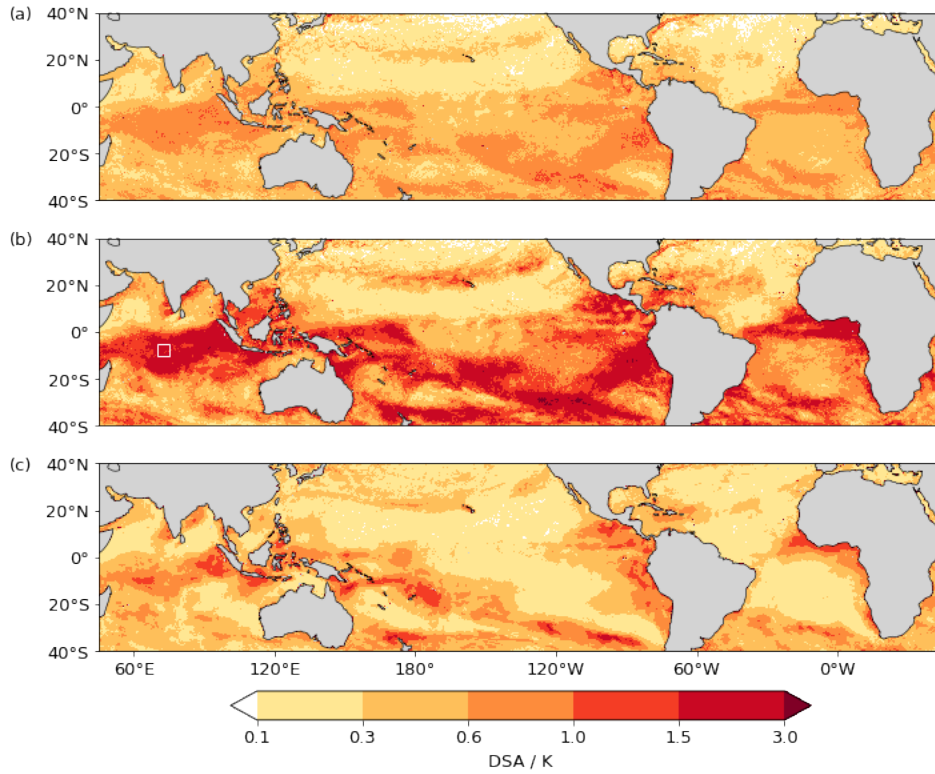


Figure 2: Magnitudes of the daily SST amplitude (max–min), averaged between 22 and 30 January 2020 in (a) S_{control} , (b) $S_{+\text{DWL}}$, and (c) ERA5. The white rectangle in (b) designates an area in the Indian ocean that is analysed in Section 3.1.

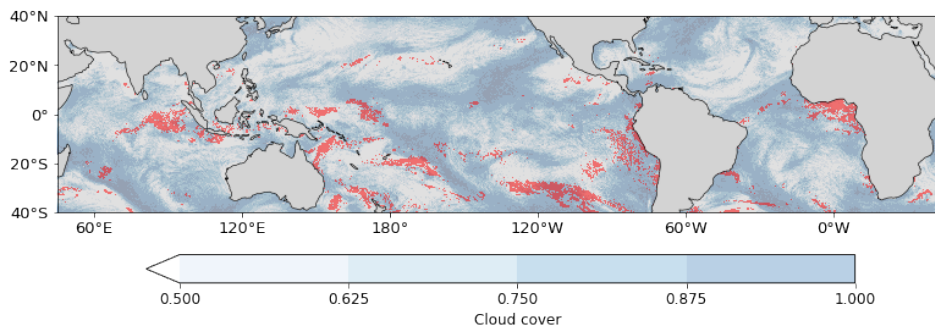


Figure 3: Cloud cover on a particular day (23 January 2020) in $S_{+\text{DWL}}$. Red areas correspond to DWL regions with DSA of over 1.5 K.

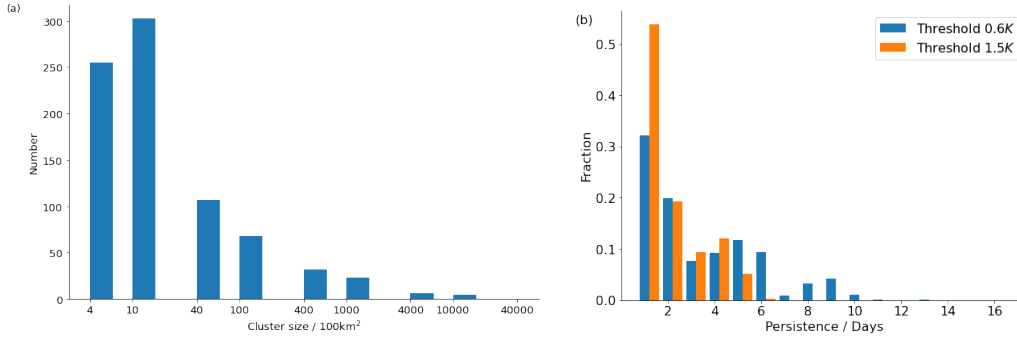


Figure 4: (a) Clusters of DWLs to the threshold of 1.5 K on a particular day (23 January 2020) ordered in a histogram of cluster sizes. (b) Normalised histogram of DWL episode lengths to different thresholds for the box 70°E–75° E and 5°S–10°S

191 lasted five days or less (see Figure 4b). Expectedly, the persistence time becomes shorter
 192 if a higher threshold for DSA is considered. This result is similar to the findings in the
 193 ERA40 forced simulation in Bellenger and Duvel (2009), where they showed that the DWL
 194 episode duration decays faster than exponentially.

195 **3.2 Structure of DWLs and preconditions for their formation**

196 For a deeper understanding of how the known properties of DWLs are captured
 197 by S_{+DWL} we focus on a study of this phenomenon in the tropical northern Atlantic re-
 198 gion off the coast of Barbados, more precisely in the box 56.5°W–59°W and 12°N–14.5°N
 199 corresponding to the region of the EUREC⁴A field campaign (Stevens et al. (2021)).

200 First, we examine the vertical structure of a DWL produced in the simulation S_{+DWL} .
 201 As shown in the anomaly profile (Figure 5), the incoming heat quickly accumulates in
 202 the upper layers during the day, as the warming of the upper layers creates a stable strat-
 203 ification if the mixing is slow, which is the case under low wind conditions. During the
 204 night, the DWL slowly dissipates until a single mixed layer is restored. As mentioned
 205 before, in this region, the heat anomalies are overestimated: a typical DSA in glider ob-
 206 servations is approximately 0.15 K (see Hohenegger et al. (2022), Figure 11c), while in
 207 S_{+DWL} in a calm period it is around 0.3 K. The time of the maximum and minimum is
 208 captured accurately compared to these observations (about 16 h LT and 8 h LT respec-
 209 tively).

Another analysis demonstrates that the dependency of DSA on insolation and sur-
 face wind observed, among others, in satellite measurements in Gentemann et al. (2003),
 are reproduced in ICON simulations as expected, namely higher DSA correlates with lower
 winds and higher downward shortwave radiation at the surface. The scatterplot in Fig-
 ure 6a shows a relationship similar to the formula

$$DSA \sim \begin{cases} U^{-3} & \text{for } U < 4\text{-}5 \text{ m s}^{-1}, \\ U^{-1} & \text{for } U > 4\text{-}5 \text{ m s}^{-1}, \end{cases}$$

210 suggested in Soloviev and Lukas (2013) for 10 m wind speed U , although the threshold
 211 appears to be located at 6–7 m s⁻¹ rather than at 4–5 m s⁻¹. Also the linear depen-
 212 dence on shortwave radiation described in Matthews et al. (2014) seems to be confirmed
 213 in S_{+DWL} (Figure 6b). In particular, the slope of the linear regression between DSA and
 214 surface downward shortwave radiation in ICON is 0.0023 K W⁻¹m², which is indeed close

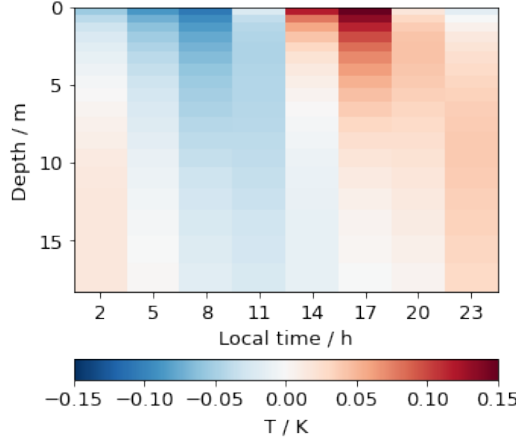


Figure 5: Sea water temperature (3 h output) averaged over 3 days over the box $56.5^{\circ}W$ - $59^{\circ}W$ and $12^{\circ}N$ - $14.5^{\circ}N$, time anomaly.

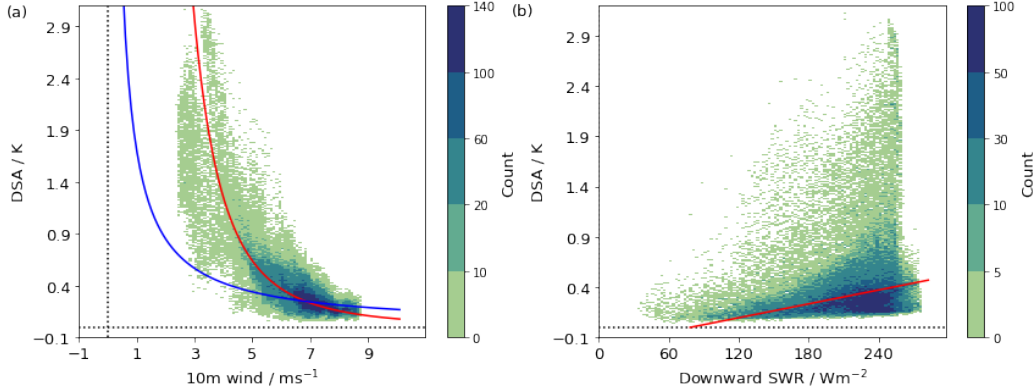


Figure 6: 2D histograms of SST amplitude and (a) 10 m wind speed as well as (b) short-wave radiation over the box $56.5^{\circ}W$ to $59^{\circ}W$ and $12^{\circ}N$ to $14.5^{\circ}N$ in S_{+DWL} . The blue and red lines in (a) indicate the interpolation of U^{-1} and U^{-3} to higher and lower wind speeds respectively. The red line in (b) is the linear regression fit between the variables.

215 to the slope of $0.0021 \text{ K W}^{-1}\text{m}^2$ found in Matthews et al. (2014). The large scattering
 216 of points in Figure 6b is caused by the joint influence of wind speed and radiation on DWLs.

217 **4 Effect of DWLs on convection**

218 The previous section shows that DWLs are frequent in the tropics, they cover large
 219 areas and persist over several days. We can therefore hypothesize that they might have
 220 an effect on atmospheric convection, either by creating horizontal air temperature gra-
 221 dients, or by enhancing the moistening of the overlying air. Moreover, as DSA in S_{+DWL}
 222 is overestimated, the effect of DWLs is expected to be too strong.

223 To assess the impact of DWLs on convective clouds, we need to compare the val-
 224 ues of relevant variables in places where DWLs develop to places where they do not devel-
 225 op. A clean way to accomplish this without having to account for other sources of vari-
 226 ability is to compare the differences between these values in S_{+DWL} and S_{control} at places

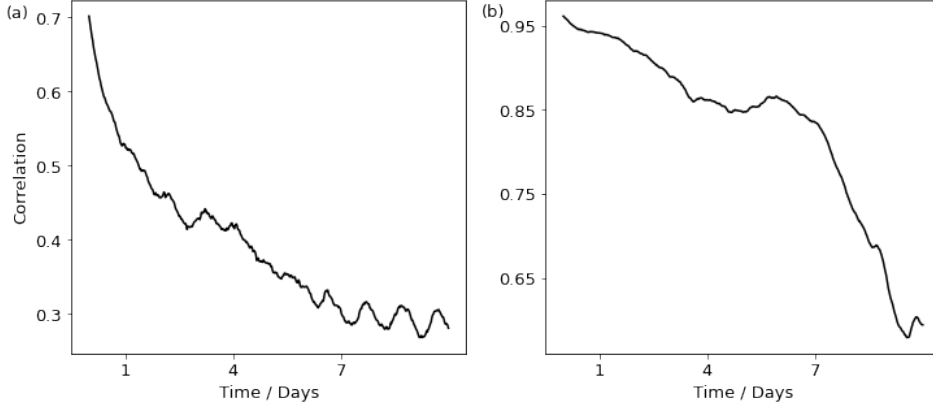


Figure 7: Temporal evolution of the global correlation between S_{control} and $S_{+\text{DWL}}$ for (a) cloud cover and (b) latent heat flux.

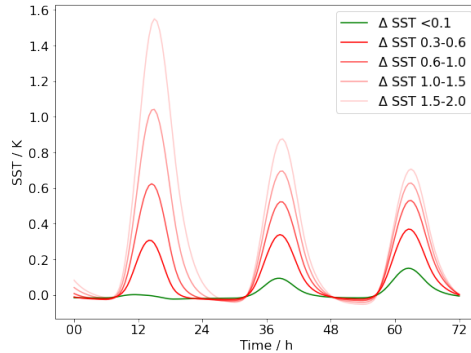


Figure 8: Time series (in local time) of $S_{+\text{DWL}} - S_{\text{control}}$ for different ΔSST .

227 where DWLs of a certain magnitude are present in $S_{+\text{DWL}}$. A key point in this analy-
 228 sis is to only include the first 4 days after the start of the simulation into the investiga-
 229 tion to ensure that the two simulations remain close and do not diverge due to the chaotic
 230 nature of the atmosphere. Figure 7 shows that both simulations indeed remain highly
 231 correlated during the first several days.

232 To conduct our analysis, we proceed as follows. The ocean is subdivided into $0.25^\circ \times$
 233 0.25° disjoint squares, and for each square the hourly maximal SST difference between
 234 $S_{+\text{DWL}}$ and S_{control} during a day, denoted by ΔSST , is computed. Based on this first day
 235 of the analysis that we also call the detection day, two groups can be formed: one called
 236 the "no DWL difference" group, where ΔSST stays below 0.1 K, and another one where
 237 ΔSST lies between certain thresholds T_1 and T_2 , which we call the "DWL difference be-
 238 tween T_1 and T_2 " group. Note that the plot of ΔSST yields a map very similar to Fig-
 239 ure 2b (Figure B1 in the Appendix), and thus can be used as a proxy for identifying DWL
 240 areas. We use this proxy from now on to cover a larger variety of cases and to obtain
 241 a cleaner comparison.

242 The subsequent analysis consists in comparing the two groups to each other, focusing
 243 on the time series of the differences in relevant variables over the days 1-3, with
 244 day 1 being the detection day, see Figure 8 for an example of the differences in SST. Sta-
 245 tistically, it is supported by t-tests for equality of means for independent samples with

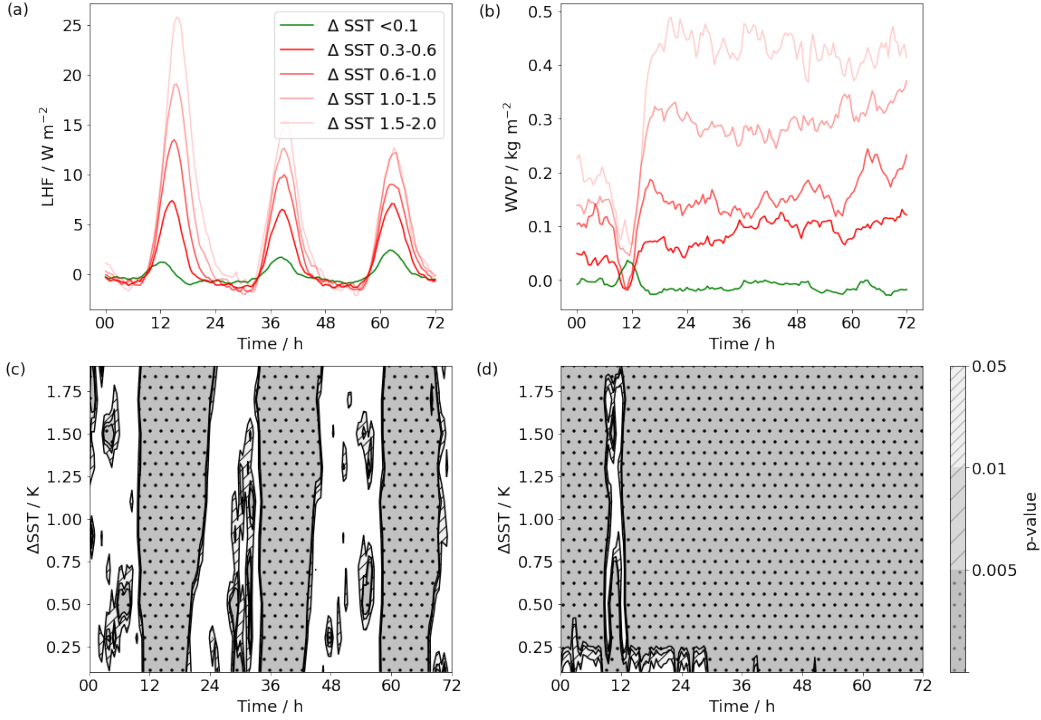


Figure 9: Time series (in local time) of $S_{+DWL}-S_{control}$ and t-test significance levels in bins of 0.1 K for LHF (a, c) and WVP (b, d). On panel c and d, white means not significant.

246 different variances. Every group with $T_2 - T_1 = 0.1$ K has at least 1695 cells, a suffi-
 247 cient number to ensure the robustness of the results. The size of the squares is chosen
 248 in accordance to the cluster sizes discussed in Section 3.1 (see Figure 4), as a mesoscale
 249 analysis is sufficient to capture a possible effect of DWLs, and also because the temper-
 250 ature and moisture changes produced by one isolated cell of $0.1^\circ \times 0.1^\circ$ are not expected
 251 to have a large effect and would be quickly mixed in the atmosphere. Moreover, we make
 252 the assumption that the effects in cloudiness are localised. Indeed, the impact of DWLs
 253 on cloud cover via moistening is a local effect, and the mesoscale circulation created by
 254 SST gradients would also result in cloud formation over DWLs. With this assumption,
 255 the samples can be treated as independent.

256 4.1 Impact on latent heat flux and related quantities

257 First we investigate whether higher ΔSST leads to more moisture in the air over
 258 DWL areas. This will help understand whether cloud formation may be impacted over
 259 DWLs. In particular, we are going to concentrate on differences in latent heat flux (LHF)
 260 and water vapor path (WVP) to measure the effects on evaporation and column moist-
 261 ening respectively, as shown in Figure 9.

262 The first observation concerning the plots (a, b) in Figure 9 is that the differences
 263 between S_{+DWL} and $S_{control}$ in the "no DWL difference" group after the detection day
 264 revolve around zero, as expected and further justifying our approach. This is not the case
 265 for the "DWL" groups. Differences are clearly appearing and are of larger magnitude,
 266 the stronger the DWL is.

267 The latent heat flux is increased when DWLs are present, with a peak around noon
 268 on every day, as expected from the daily cycle in SST. WVP is always higher over DWLs.
 269 The difference decreases in the morning hours of the detection day and increases rapidly
 270 thereafter. The dip could be caused either by a dip in LHF, by an increase of precipi-
 271 tation or by a weakening in convergence of moisture. As LHF is increased and there is
 272 no excessive rain over DWLs (not shown), the dip must be due to weaker convergence,
 273 which might be caused by a weakening of surface wind required for DWL formation. The
 274 increase of WVP after 12 h LT reflects the increase in moisture due to increased LHF.
 275 One can trace the propagation of the moisture response to DWLs in Figure 9, since the
 276 onset and duration times of the effects are different: while LHF reacts immediately and
 277 is tied directly to differences in temperature (see Figure 8), the effect on WVP is delayed
 278 by several hours and persists over the following days without losing its magnitude.

279 Figure 9(c, d) confirms that the differences observed visually are highly significant
 280 even on the third day and even for small Δ SST with p-values smaller than 0.005, except
 281 for the nighttime values of LHF. However, an important point is that the absolute dif-
 282 ferences are rather small, especially for smaller Δ SST: For instance, for Δ SST between
 283 0.6 K and 1.0 K, the peak of LHF is below 15 W m^{-2} and WVP is below 0.2 kg m^{-2} .
 284 One can compare these values with global averages of the two quantities over the ocean,
 285 which are ca. 130 W m^{-2} for LHF and ca. 34.6 kg m^{-2} for WVP. The order of magni-
 286 tude of LHF changes is similar to that found in the single column configuration in Voltaire
 287 et al. (2022).

288 4.2 Impact on cloudiness

289 The variables we consider for analysing the impact of DWLs on clouds are cloud
 290 cover (CC) and cloud liquid water (CLW).

291 The responses of CC and CLW shown in Figure 10 are very similar to each other.
 292 The "no DWL difference" time series is fluctuating around zero after the detection day,
 293 but on the detection day itself there is a peak at midday. In contrast, the DWLs regions
 294 exhibit dips at the same time, and the magnitude of these dips is positively correlated
 295 with the Δ SST amplitude (see Figure 10(a, b) and Figure 10(e, f)). This illustrates the
 296 prerequisite for DWLs to exist mentioned in Section 3.1: The appearance of DWLs is
 297 generally favored by a lower cloud amount. Subsequently we can observe the cloud re-
 298 sponse to the formation of DWLs on the detection day: after about 12 h LT, the differ-
 299 ence between S_{+DWL} and $S_{control}$ in both CC and CLW over DWLs starts to grow, and
 300 by 15 h LT both simulations have the same cloud amount. This growth is statistically
 301 significant starting from an SST amplitude of 0.3 K, and the effect persists longer for
 302 higher values of Δ SST, namely until 20 h LT for Δ SST of 1.5-2.0 K and until 18 h LT
 303 for Δ SST of 0.3-1.0 K for CC. Moreover, the effect seems to last longer for CLW, although
 304 the values of both variables fall back below the zero line already during the night. In to-
 305 tal, the increase of cloud following the formation of a DWL lasts up to 5-6 h.

306 A behaviour similar to the first day, that is, less CC and CLW in S_{+DWL} compared
 307 to $S_{control}$ in the morning and rise of these quantities in S_{+DWL} in the afternoon, can be
 308 observed also on the second and third day after the detection day (Figure 10(a, b)), how-
 309 ever, the deviation is barely significant: most of the time, the p-value is above 0.05, es-
 310 pecially for higher values of Δ SST (Figure 10(c, d)). This means that the increase of the
 311 quantities is often not homogeneous enough to be interpreted as systematic (see Figure
 312 10(c, d)). A crucial factor here is the absolute magnitude of the differences: In extreme
 313 cases, for Δ SST between 1.5 and 2.0 K, the deviation of CC reaches 0.03 and that of CLW
 314 0.02 kg m^{-2} on the detection day. On the following day the corresponding maximal val-
 315 ues fall to 0.01 and 0.01 kg m^{-2} , while the averages are 0.001 and 0.002 kg m^{-2} respec-
 316 tively (see Figure 10(a, b)). We can compare those to the average values of CC and CLW
 317 over DWLs, 0.65 for CC and 0.11 kg m^{-2} for CLW. The average increase in CLW is about

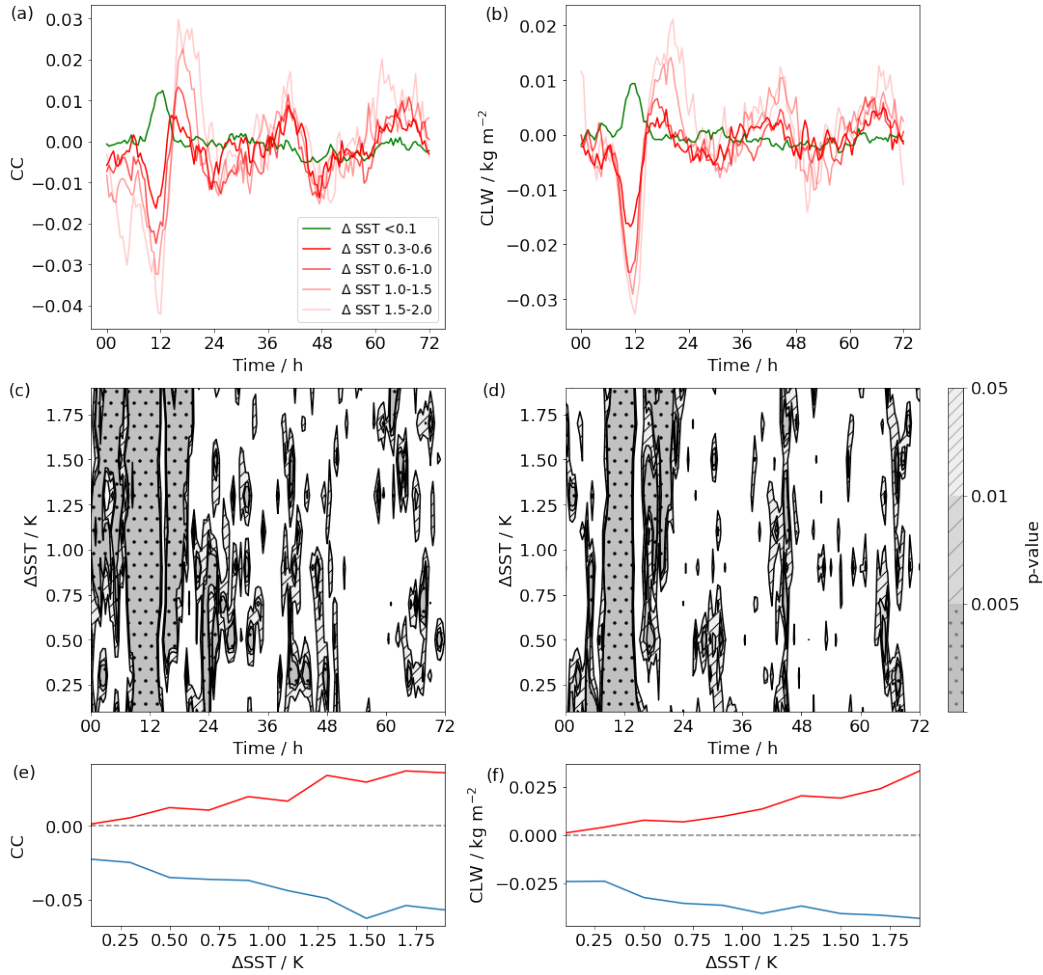


Figure 10: Time series (in local time) of $S_{+DWL} - S_{control}$, t-test significance levels in bins of 0.1 K, and maximal (red) and minimal (blue) value of the deviation on the detection day for CC (a, c, e) and CLW (b, d, f).

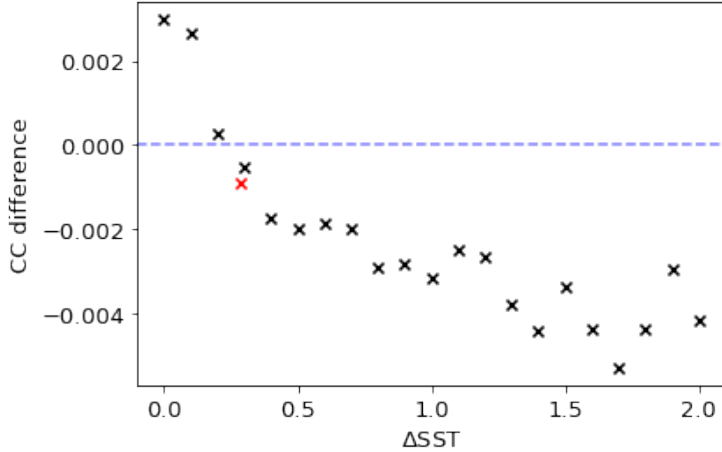


Figure 11: Daily mean CC differences ($S_{+DWL} - S_{control}$) as a function of ΔSST (black crosses). The red cross is the average CC difference against the average ΔSST .

318 1% and the increase in CC is about 0.2% on the day following even very large ΔSST .
 319 We can therefore conclude that the effect on the cloud water content is higher than the
 320 contribution of DWLs to cloud cover change, but the effects are very small.

321

322 The morning/midday dip of CC and CLW over DWLs even overcompensates the
 323 subsequent rise of these quantities. Figure 11 shows mean CC differences between S_{+DWL}
 324 and $S_{control}$ as a function of ΔSST on the detection day. For ΔSST above 0.3 K the sim-
 325 ulation S_{+DWL} has lower values of CC than $S_{control}$, and only for ΔSST below 0.3 K the
 326 reverse is true, such that on average, S_{+DWL} has slightly less cloud than $S_{control}$. The
 327 effect of DWLs appears to be dominated by the variability of the model. All in all, we
 328 can conclude that DWLs do not increase the global mean of cloud cover or cloud liquid
 329 water path.

330 We continue the analysis by looking at deep and shallower clouds separately, as one
 331 might expect to see more effects associated with one type of clouds. We differentiate be-
 332 tween deep and shallow clouds by taking the outgoing longwave radiation at the top of
 333 the atmosphere of 240 W m^{-2} as a threshold. This value is mentioned in Fu et al. (1990)
 334 as the threshold often used to identify deep convection. While the figures for shallower
 335 clouds are very similar to Figure 10 (not shown), the deviation for CLW in deep clouds
 336 is somewhat larger, up to 0.03 kg m^{-2} on the detection day. As shown in Figure 12a for
 337 CC, the effects, despite being a bit larger, remain very small and do not exhibit system-
 338 atic significance (Figure 12c). Considering precipitation as an additional possibility to
 339 see an impact of DWLs (Figure 12(b, d)), we see that there is no sufficient evidence to
 340 attribute the fluctuations of precipitation, even for higher values of ΔSST , to anything
 341 more than chance.

342 The last question that we want to investigate is to what extent the presence of DWLs
 343 might affect the diurnal cycle of convection. We focus on the example of the EUREC⁴A
 344 field campaign, which took place in the northern tropical Atlantic. For this region the
 345 diurnal cycle of shallow convection has been studied in great detail in Vial et al. (2019).
 346 In particular, it has been shown there that, in observations as well as in large-eddy sim-
 347 ulations (LES), the cloud cover peaks during the day, which might make it more suscep-
 348 tible to SST in comparison to other regions. In our case, both S_{+DWL} and $S_{control}$ over-

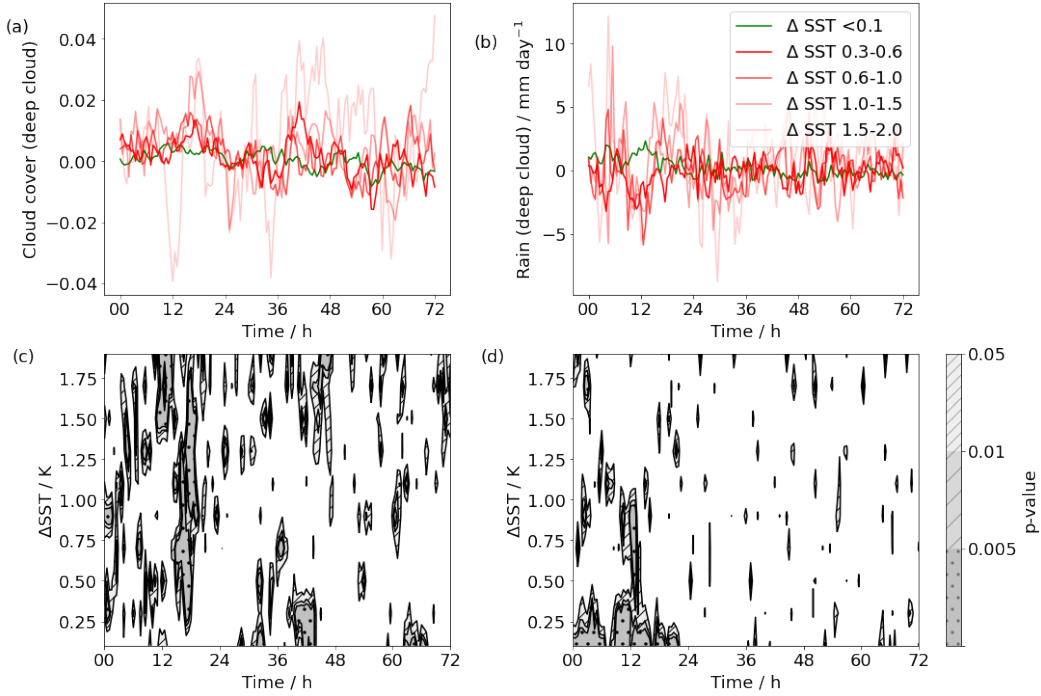


Figure 12: As Figure 9, but for CC (a, c) and precipitation (b, d) associated with deep convection.

349 estimate the CC found in observations by a factor of 2, as was expected from the res-
 350 olution sensitivity study in Vial et al. (2019), but capture perfectly the time structure
 351 as well as the amplitude of the cycle: minimum between 12 and 15 LT, maximum at 2
 352 LT, amplitude of about 0.1 (Figure 13), in good agreement with observations in Vial et
 353 al. (2019). The increase in CC resulting from the appearance of DWLs occurs in the late-
 354 afternoon. If anything, CC slightly decreases at other times. Both effects taken together
 355 tend to slightly reduce the diurnal amplitude. The fact that DWLs only have a small
 356 influence on the diurnal cycle of CC is consistent with the study in Vial et al. (2019) that
 357 reproduced the main features of the cycle in LES despite using fixed SST.

358 5 Discussion and conclusions

359 By introducing thin vertical levels into the global coupled ICON model, we could
 360 directly resolve diurnal warm layers (DWLs) and assess their impact on the atmosphere.
 361 The simulations employed a grid spacing of 5 km, both in the atmosphere and ocean,
 362 so that ocean mesoscale eddies and atmospheric convection can be resolved explicitly.
 363 The DWLs produced by the simulation reproduce the physical features known from ob-
 364 servations and limited area decameter simulations, but the magnitude of the daily SST
 365 fluctuations is exaggerated in comparison to reanalysis, by about a factor of two.

366 The increase in the amplitude of the diurnal cycle of SST in regions with diurnal
 367 warm layers leads to a corresponding increase in latent heat flux (LHF) and water va-
 368 por path (WVP). The effects are significant, even on days 2 and 3 following the detec-
 369 tion of a diurnal warm layer, but the values are small: 7 W m⁻² difference in LHF and
 370 0.1 kg m⁻² difference in WVP for a SST difference of 0.6 K. In the late-afternoon of the
 371 detection day, cloud cover (CC) and cloud liquid water (CLW) content also increase, but
 372 the effects are small and lose statistical significance within 5-6 hours of appearance. What

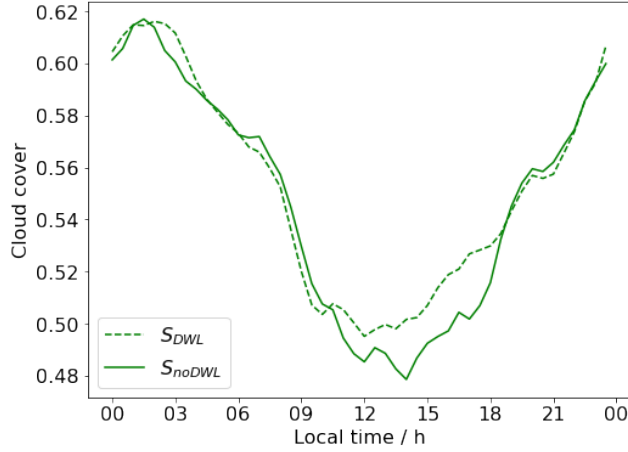


Figure 13: Diurnal cloud cover cycle in the box 56.5°W to 59°W and 12°N to 14.5°N, composite over 30 days.

373 is however significant is a decrease in cloud cover and liquid water content on the day
 374 of detection, around noon. This expresses the fact that diurnal warm layers favorably
 375 form in areas of low cloud cover, and hence high insolation. This effect compensates the
 376 subsequent increase. All in all, resolving diurnal warm layers does not affect the mean
 377 cloud cover over tropical oceans.

378 The amplitude of the observed differences in LHF is similar to findings in Voldoire
 379 et al. (2022), and the impact on cloud cover shows that convection over DWLs is enhanced,
 380 as it is claimed in the observation study of de Szoeke et al. (2021). Moreover, the small
 381 influence of DWLs on the CC cycle in the tropical Atlantic supports the results in Vial
 382 et al. (2019). A surprising and unprecedented finding of our study is the impact of DWLs
 383 on convection remains small even for a strongly enhanced daily SST amplitude over this
 384 particular region as well as globally.

385 We finish the discussion by focusing on the implications and limitations of our study.
 386 Regarding the question of the importance of DWLs in models, one needs to differenti-
 387 ate between the local and the overall impact. In our exemplary study in the northern
 388 tropical Atlantic, the presence of DWLs can reduce the amplitude of the diurnal cycle
 389 of the cloud cover by up to 10% (see Figure 13). In some specific cases with extraordi-
 390 narily high DSA, DWLs might indeed play a role. However, this remains a rare phenomenon.

391 The analysis in this manuscript only concerns short-term effects of DWLs. How-
 392 ever, it is known that the mean SST increases in DWL areas (Bellenger and Duvel (2009)).
 393 Therefore, inclusion of DWLs will have a long-term influence on the energy budget that
 394 is not treated here, but at least for short-term effects, our study demonstrates that DWLs
 395 do not have a global and significant impact.

396

Appendix A Vertical resolution of the simulations

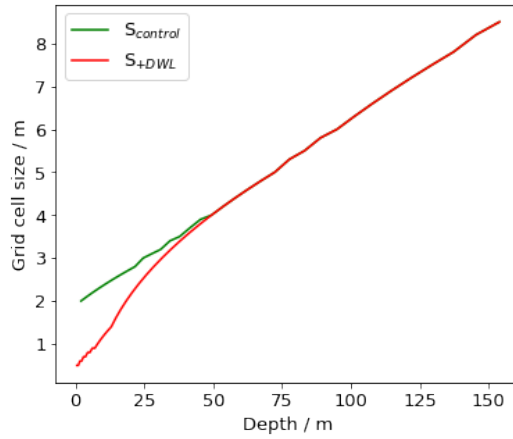


Figure A1: Layer thicknesses for S_{+DWL} and $S_{control}$

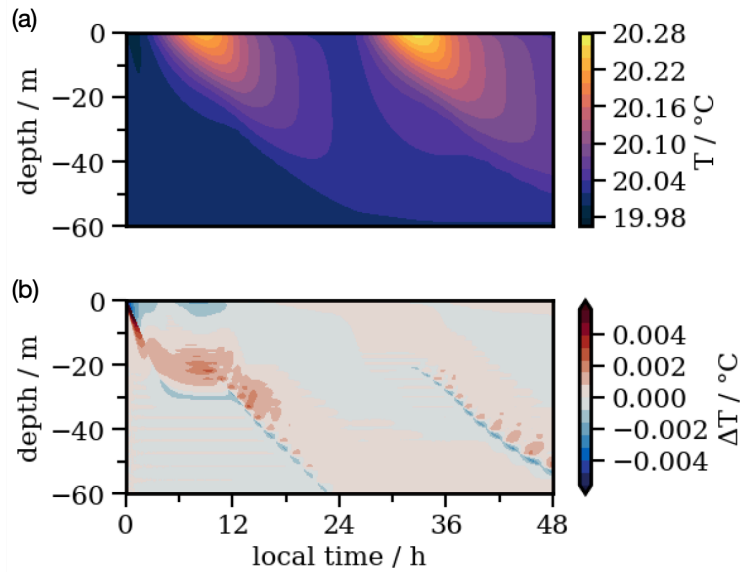
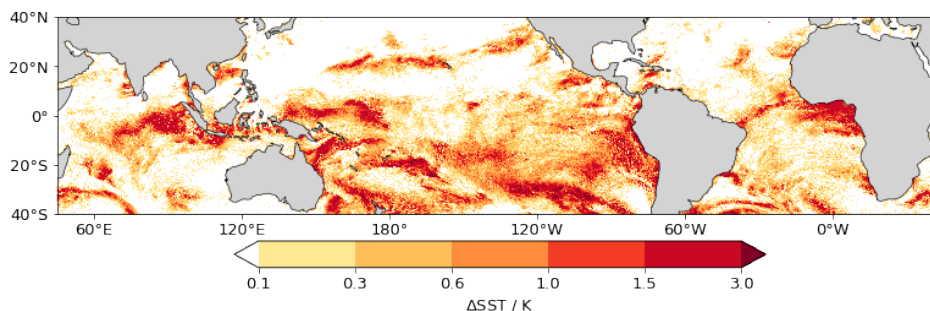


Figure A2: (a) As in Figure 1, but with uniform 0.1 m thick vertical layers. (b) Difference between the temperature profiles in Figure 1 and (a).

397

Appendix B Average ΔSST as proxy for DSA

Figure B1: Δ SST on detection day.

Appendix C Open Research

Detailed information concerning the ICON model is contained in the publication Hohenegger et al. (2022). The ocean model GOTM is documented in Umlauf et al. (2005) and can be installed from <https://gotm.net>. The ERA5 dataset used in this study has been provided by the Climate Data Store.

Acknowledgments

This work used resources of the Deutsches Klimarechenzentrum (DKRZ) granted by its Scientific Steering Committee (WLA) under project ID bm1253. The authors gratefully acknowledge the support of the DFG-funded collaborative research centre TRR181 "Energy Transfers in Atmosphere and Ocean".

References

- Bellenger, H., & Duvel, J.-P. (2009). An analysis of tropical ocean diurnal warm layers. *Journal of Climate*, *22*(13), 3629 - 3646. Retrieved from <https://journals.ametsoc.org/view/journals/clim/22/13/2008jcli2598.1.xml> doi: 10.1175/2008JCLI2598.1
- Brilouet, P.-E., Redelsperger, J.-L., Bouin, M.-N., Couvreur, F., & Lebeaupin Brossier, C. (2021). A case-study of the coupled ocean-atmosphere response to an oceanic diurnal warm layer. *Quarterly Journal of the Royal Meteorological Society*, *147*(736), 2008-2032. Retrieved from <https://rmets.onlinelibrary.wiley.com/doi/abs/10.1002/qj.4007> doi: <https://doi.org/10.1002/qj.4007>
- de Szoeko, S. P., Marke, T., & Brewer, W. A. (2021). Diurnal ocean surface warming drives convective turbulence and clouds in the atmosphere. *Geophysical Research Letters*, *48*(4), e2020GL091299. Retrieved from <https://agupubs.onlinelibrary.wiley.com/doi/abs/10.1029/2020GL091299> (e2020GL091299 2020GL091299) doi: <https://doi.org/10.1029/2020GL091299>
- Fu, R., Genio, A. D. D., & Rossow, W. B. (1990). Behavior of deep convective clouds in the tropical pacific deduced from isccp radiances. *Journal of Climate*, *3*(10), 1129 - 1152.
- Gentemann, C. L., Donlon, C. J., Stuart-Menteth, A., & Wentz, F. J. (2003). Diurnal signals in satellite sea surface temperature measurements. *Geophysical Research Letters*, *30*(3). Retrieved from <https://agupubs.onlinelibrary.wiley.com/doi/abs/10.1029/2002GL016291> doi: <https://doi.org/10.1029/2002GL016291>
- Hohenegger, C., Korn, P., Linardakis, L., Redler, R., Schnur, R., Adamidis, P.,

- 433 ... Stevens, B. (2022). Icon-sapphire: simulating the components of the
 434 earth system and their interactions at kilometer and subkilometer scales.
 435 *Geoscientific Model Development Discussions*, 2022, 1–42. Retrieved
 436 from <https://gmd.copernicus.org/preprints/gmd-2022-171/> doi:
 437 10.5194/gmd-2022-171
- 438 Hohenegger, C., Kornblueh, L., Klocke, D., Becker, T., Cioni, G., Engels, J. F., ...
 439 Stevens, B. (2020). Climate statistics in global simulations of the atmosphere,
 440 from 80 to 2.5 km grid spacing. *Journal of the Meteorological Society of Japan*.
 441 *Ser. II*, 98(1), 73-91. doi: 10.2151/jmsj.2020-005
- 442 Kawai, Y., & Wada, A. (2007). Diurnal sea surface temperature variation and
 443 its impact on the atmosphere and ocean: A review. *Journal of Oceanog-*
 444 *raphy*, 63(5), 721–744. Retrieved from [https://doi.org/10.1007/](https://doi.org/10.1007/s10872-007-0063-0)
 445 [s10872-007-0063-0](https://doi.org/10.1007/s10872-007-0063-0) doi: 10.1007/s10872-007-0063-0
- 446 Matthews, A. J., Baranowski, D. B., Heywood, K. J., Flatau, P. J., & Schmidtko,
 447 S. (2014). The surface diurnal warm layer in the indian ocean dur-
 448 ing cindy/dynamo. *Journal of Climate*, 27(24), 9101 - 9122. Retrieved
 449 from [https://journals.ametsoc.org/view/journals/clim/27/24/](https://journals.ametsoc.org/view/journals/clim/27/24/jcli-d-14-00222.1.xml)
 450 [jcli-d-14-00222.1.xml](https://journals.ametsoc.org/view/journals/clim/27/24/jcli-d-14-00222.1.xml) doi: 10.1175/JCLI-D-14-00222.1
- 451 Price, J. F., Weller, R. A., & Pinkel, R. (1986). Diurnal cycling: Observations
 452 and models of the upper ocean response to diurnal heating, cooling, and
 453 wind mixing. *Journal of Geophysical Research: Oceans*, 91(C7), 8411-8427.
 454 Retrieved from [https://agupubs.onlinelibrary.wiley.com/doi/abs/](https://agupubs.onlinelibrary.wiley.com/doi/abs/10.1029/JC091iC07p08411)
 455 [10.1029/JC091iC07p08411](https://doi.org/10.1029/JC091iC07p08411) doi: <https://doi.org/10.1029/JC091iC07p08411>
- 456 Soloviev, A., & Lukas, R. (2013). *The near-surface layer of the ocean: Structure, dy-*
 457 *namics and applications*. Springer Netherlands. Retrieved from [https://books](https://books.google.de/books?id=_4zHBAAAQBAJ)
 458 [.google.de/books?id=_4zHBAAAQBAJ](https://books.google.de/books?id=_4zHBAAAQBAJ)
- 459 Stevens, B., Bony, S., Farrell, D., Ament, F., Blyth, A., Fairall, C., ... Zöger,
 460 M. (2021). Eurec⁴a. *Earth System Science Data*, 13(8), 4067–4119. Re-
 461 trieved from <https://essd.copernicus.org/articles/13/4067/2021/> doi:
 462 10.5194/essd-13-4067-2021
- 463 Sverdrup, H., Johnson, M., & Fleming, R. (1942). *The oceans, their physics,*
 464 *chemistry, and general biology*. Prentice-Hall, Incorporated. Retrieved from
 465 <https://books.google.de/books?id=h74gAAAAMAAJ>
- 466 Umlauf, L., Bolding, K., & Burchard, H. (2005). *GOTM – scientific documentation,*
 467 *version 3.2* (Vol. 63). Leibniz-Institute for Baltic Sea Research, Warnemünde,
 468 Germany. Retrieved from <https://gotm.net/manual/stable/pdf/a4.pdf>
- 469 Vial, J., Vogel, R., Bony, S., Stevens, B., Winker, D. M., Cai, X., ... Brogniez,
 470 H. (2019). A new look at the daily cycle of trade wind cumuli. *Jour-*
 471 *nal of Advances in Modeling Earth Systems*, 11(10), 3148-3166. Retrieved
 472 from [https://agupubs.onlinelibrary.wiley.com/doi/abs/10.1029/](https://agupubs.onlinelibrary.wiley.com/doi/abs/10.1029/2019MS001746)
 473 [2019MS001746](https://doi.org/10.1029/2019MS001746) doi: <https://doi.org/10.1029/2019MS001746>
- 474 Voltaire, A., Roehrig, R., Giordani, H., Waldman, R., Zhang, Y., Xie, S., & Bouin,
 475 M.-N. (2022). Assessment of the sea surface temperature diurnal cycle in
 476 cnrm-cm6-1 based on its 1d coupled configuration. *Geoscientific Model Devel-*
 477 *opment*, 15(8), 3347–3370. Retrieved from [https://gmd.copernicus.org/](https://gmd.copernicus.org/articles/15/3347/2022/)
 478 [articles/15/3347/2022/](https://gmd.copernicus.org/articles/15/3347/2022/) doi: 10.5194/gmd-15-3347-2022
- 479 Wick, G. A., & Castro, S. L. (2020). Assessment of extreme diurnal warming in
 480 operational geosynchronous satellite sea surface temperature products. *Remote*
 481 *Sensing*, 12(22). Retrieved from [https://www.mdpi.com/2072-4292/12/22/](https://www.mdpi.com/2072-4292/12/22/3771)
 482 [3771](https://www.mdpi.com/2072-4292/12/22/3771) doi: 10.3390/rs12223771